Simulation of flexural-gravity wave propagation for elastic plates in shallow water using energy-stable finite difference method with weakly enforced boundary and interface conditions

Nurbek Tazhimbetov^{a,*}, Martin Almquist^c, Jonatan Werpers^c, Eric M. Dunham^{a,b}

^aInstitute for Computational and Mathematical Engineering, Stanford University, Stanford, CA, USA

^bDepartment of Geophysics, Stanford University, Stanford, CA, USA

^cDepartment of Information Technology, Uppsala University, Uppsala, Sweden

Abstract

We introduce an energy stable, high-order-accurate finite difference approximation of the dynamic, pure bending Kirchhoff plate equations for complex geometries and spatially variable properties. We utilize the summation-by-parts (SBP) framework to discretize the biharmonic operator with variable coefficients, with attention given to free and clamped boundary conditions and corner conditions. Energy conservation is established by combining SBP boundary closures with weak enforcement of the boundary and interface conditions using a penalty (simultaneous approximation term, SAT) technique. Then we couple the plate equations to the shallow water equations to study flexural-gravity wave propagation, and prove that the semi-discrete system of equations is self-adjoint. We demonstrate the stability and accuracy properties of the method on curvilinear multiblock grids using the method of manufactured solutions. The method, which we provide in an open-source code, is then used to model ocean wave interactions with the Thwaites Glacier and Pine Island Ice Shelf in the Amundsen Sea off the coast of West Antarctica.

Keywords: biharmonic operators with variable coefficients, plate equation, curvilinear grids, summation by parts, finite difference

PACS: 02.30.Jr, 02.70.-c, 46.15.-x, 46.70.De

2010 MSC: 65M06, 65M12, 35L53, 74B05, 74K20

1. Introduction

In this work, we consider numerical solution for pure bending of plates in complex geometries with spatially variable coefficients. The equations are based on the Kirchhoff-Love model of isotropic plates, which is a two-dimensional mathematical model for flexure and bending stresses in a thin plate for which the plate thickness is much smaller than the plate

Preprint submitted to Journal of Computational Physics

June 3, 2022

^{*}Corresponding author

Email addresses: nurbek@stanford.edu (Nurbek Tazhimbetov), martin.almquist@it.uu.se (Martin Almquist), jonatan@werpers.com (Jonatan Werpers), edunham@stanford.edu (Eric M. Dunham)

dimensions. This plate model is an extension of the one-dimensional Euler-Bernoulli beam model. The governing equation of the pure bending of plates is a linear partial differential equation (PDE) that is fourth order in two-dimensional space and second order in time.

The main motivation for our work is to study the impact of long wavelength ocean waves (storm swell, tsunamis, infragravity waves, and even tidal forcing) on ice shelves. Recent studies, some of which are based on data from broadband seismic arrays in Antarctic ice shelves, reveal the extent of flexure caused by ocean waves, which in some cases has been linked to the growth of rifts, fractures, and even break-up of ice shelves [18], [5], [4], [20].

Quantitative model-based studies of this problem are based on the hydroelastic framework for ice shelves originally developed by [9], [10], and which is widely applied in the sea ice community [8]. In this framework, the ice shelf is modeled as a thin elastic plate floating on an inviscid, incompressible fluid layer (the ocean). While the governing equations can be solved analytically in very simple geometries, numerical solution is required for spatially variable properties (including variable water depth and ice thickness) and complex geometries in map view. Most models restrict attention to a 2D vertical cross-section, with the governing equations solved using eigenfunction expansions and related semi-analytical methods [8, 33, 31, 25], the finite element method [27, 11, 13], and the finite difference method [23]. Of particular note is the extension of this work into 3D by [32] to account for the spatially variable ice thickness and complex geometries characteristic of real ice shelves. Most of these studies utilize the shallow water approximation for the ocean, though this limits application to long period waves [12].

In this study, we utilize the high-order, summation-by-parts finite difference method to solve the 2D (map view) problem with variable coefficients and complex geometries, thereby extending earlier work using similar difference operators [23]. In general, high-order finite difference methods are very powerful for wave-propagation problems involving propagation over many wavelengths due to excellent numerical dispersion properties [15]. The major drawbacks of high-order finite difference methods are handling complex geometries and obtaining a stable boundary treatment.

The summation-by-parts-simultaneous-approximation-term (SBP-SAT) method is a robust and well-proven framework for solving well-posed initial boundary value problems. This method utilizes spatial-derivative operators that satisfy a summation-by-parts (SBP) property [16] with boundary conditions implemented using a penalty technique known as the the simultaneous-approximation-term (SAT) method [6]. Among the growing literature using SBP-SAT methods, we highlight review articles [34, 7] and a few recent studies on wave propagation involving second-order PDEs with variable coefficients arising in continuum mechanics [28, 1, 2]. While the SBP-SAT method has primarily been used for first and second derivatives in space, it has recently been extended to third and fourth derivatives [22], [24], [23], but only in either 1D or on Cartesian grids. An important extension, which we pursue here, is to extend this work to curvilinear, multiblock grids, in the specific context of the variable coefficient plate equation coupled to the variable coefficient shallow water equation.

The rest of the paper is organized as follows. Section 2 introduces our notational conventions and Section 3 covers the plate equation. We introduce SBP operators in Section 4, and combine them with proper SATs to construct energy-stable self-adjoint schemes for the

plate equation with free boundary conditions combined with corner conditions and clamped boundary conditions in Section 6. In Section 5, interface SATs for grid-block couplings are derived. In Section 7, we couple the plate equation to the shallow water equation to model the interaction of ice shelves with ocean waves. In Section 8, we present numerical experiments, starting with a convergence study using the method of manufactured solutions. We then apply the method to study wave-ice shelf interactions in the Amundsen Sea region of West Antarctica, which contains the Thwaites Ice Shelf Tongue and Pine Island Glacier. Lastly, we conclude with summaries in Section 9.

2. Notation conventions

In this work, we consider scalar, vector, and tensor fields in \mathbb{R}^d (with d=2 in most cases), with summation implied over repeated subscript indices, e.g.,

$$u_i v_i = \sum_{i=1}^d u_i v_i. \tag{1}$$

The L^2 inner product for bounded domains $\Omega \in \mathbb{R}^d$ is

$$(u,v)_{\Omega} = \int_{\Omega} uv \, d\Omega \tag{2}$$

and for integrals over a surface $\partial\Omega$, we write

$$(u,v)_{\partial\Omega} = \int_{\partial\Omega} uv \, dS,\tag{3}$$

which is a bilinear form.

When multiple boundary segments are present, we introduce a superscript α , defining C^{α} as subsets of $\partial\Omega$ such that $\bigcup_{\alpha}C^{\alpha}=\partial\Omega$ and two adjacent segments meet at one point. Let us call it a corner point. Then C^{α} denotes the smooth segment between beginning and ending corner points C_0^{α} and C_1^{α} , respectively (see Fig. 1b).

The integrals inherit the summation convention too, i.e.,

$$(u_i, v_i)_X = \sum_{i=1}^d (u_i, v_i)_X,$$
 (4)

where X is either Ω or $\partial\Omega$. The summation convention applies only to the following indices: i, j, k and their uppercase counterparts.

Boldface font is used for vectors \mathbf{u} , whose elements approximate some scalar field evaluated on the grid, and similarly for vector and tensor fields. We will later define discrete inner products and use the summation convention in the discrete setting too, so that

$$(\mathbf{u}_i, \mathbf{v}_i) = \sum_{i=1}^d (\mathbf{u}_i, \mathbf{v}_i), \tag{5}$$

for example. For all spatially variable coefficients, the same symbol will be used in the discrete case, too, which then is understood to denote a diagonal matrix with the values of that coefficient on the diagonal. We regard the outward unit normal and unit tangent vectors as variable coefficients that take non-zero values only at boundary points. In the discrete space, the values of these unit vectors at the corner and edge points vary depending on context. When integrating over a face, these values are understood to denote the unit normal and the unit tangent to that face even at edge and corner points. The surface area element inherits the same convention.

Finally, let W and Φ be subsets of $L^2(\Omega)$, where W and Φ are the primal and the dual spaces, respectively. The adjoint $\mathcal{L}^{\dagger}: \Phi \to L^2(\Omega)$ of a linear operator $\mathcal{L}: W \to L^2(\Omega)$ satisfies

$$(\phi, \mathcal{L}w)_{\Omega} = (\mathcal{L}^{\dagger}\phi, w)_{\Omega} \quad \forall w \in \mathcal{W}, \phi \in \Phi.$$
 (6)

The operator \mathcal{L} is said to be self-adjoint if $\mathcal{L}^{\dagger} = \mathcal{L}$, which implies that $\Phi = \mathcal{W}$ [30].

3. Equations of pure bending of plates

Let $\{\vec{E}_I\}$ denote an orthonormal basis in \mathbb{R}^d , $\vec{X} = X_I \vec{E}_I$ and $\partial_I = \partial/\partial X_I$. In this study, we consider $\Omega \subset \mathbb{R}^2$, a bounded domain with outward unit normal $\hat{N} = n_I \vec{E}_I$ and counter-clockwise unit tangent $\hat{T} = \tau_I \vec{E}_I$ to the boundary $\partial \Omega$.

The governing equations for dynamic, pure bending of plates in the absence of body forces and boundary forcing are (Chapter 3 in [29])

$$m\ddot{w} - \partial_J \partial_I M_{IJ} w = 0,$$
 $\vec{X} \in \Omega,$ $t \ge 0,$ (7a)

$$Lw = 0,$$
 $\vec{X} \in \partial\Omega,$ $t \ge 0.$ (7b)

where the moments are given by the operator

$$M_{IJ} = -\nu B \delta_{IJ} \partial_K \partial_K - (1 - \nu) B \partial_I \partial_J, \tag{8}$$

 δ_{IJ} is the Kronecker delta, $w(\vec{X},t)$ is the vertical displacement, $m(\vec{X})$ is mass per unit area (vertically integrated plate density), $B(\vec{X})$ is the bending stiffness, $\nu(\vec{X})$ is Poisson's ratio, and the linear operator L represents well-posed boundary conditions.

3.1. Weak form and energy balance

Multiplying (7a) by ψ and integrating over Ω gives us

$$(m\psi, \ddot{w})_{\Omega} - (\psi, \partial_J \partial_I M_{IJ} w)_{\Omega} = 0. \tag{9}$$

Integrating the second term by parts yields

$$(\psi, \partial_J \partial_I M_{IJ} w)_{\Omega} = (\psi, n_J \partial_I M_{IJ} w)_{\partial\Omega} - (n_I \partial_J \psi, M_{IJ} w)_{\partial\Omega} + (\partial_I \partial_J \psi, M_{IJ} w)_{\Omega}, \qquad (10)$$

where the boundary terms are

$$BT = (\psi, n_J \partial_I M_{IJ} w)_{\partial\Omega} - (n_I \partial_J \psi, M_{IJ} w)_{\partial\Omega}.$$
(11)

We rewrite the last boundary integral by separating derivatives in the normal and tangential directions using

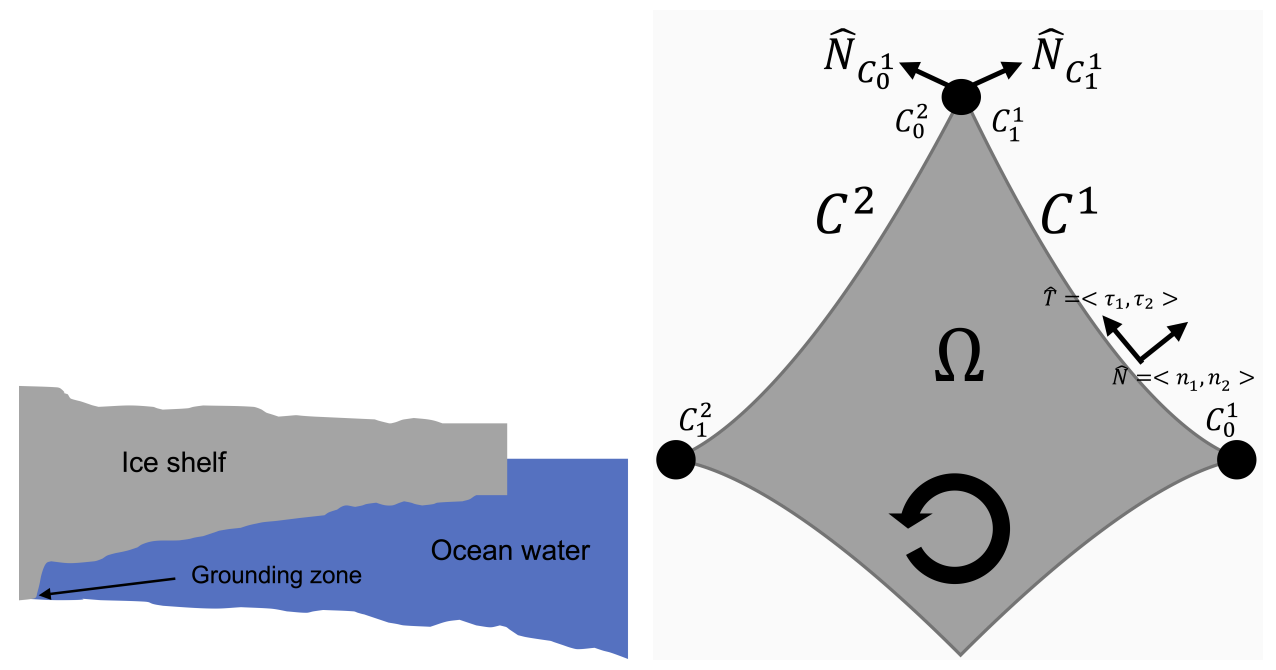
$$\partial_J = n_J n_K \partial_K + \tau_J \tau_K \partial_K, \tag{12}$$

such that

$$(n_I \partial_J \psi, M_{IJ} w)_{\partial\Omega} = (\partial_J \psi, n_I M_{IJ} w)_{\partial\Omega}$$

$$= (n_J n_K \partial_K \psi, n_I M_{IJ} w)_{\partial\Omega} + (\tau_J \tau_K \partial_K \psi, n_I M_{IJ} w)_{\partial\Omega}$$

$$= (n_K \partial_K \psi, n_J n_I M_{IJ} w)_{\partial\Omega} + (\tau_K \partial_K \psi, \tau_J n_I M_{IJ} w)_{\partial\Omega}.$$
(13)



(a) Cross-sectional view of the ice shelf-ocean water domain

(b) Corner condition is enforced when the two normal vectors at a point belonging to two boundary segments are not equal: $\hat{N}_{C_1^1} \neq \hat{N}_{C_2^0}$. Note that the direction of integration is counter-clockwise.

Figure 1: Cross-sectional view of the domain and treatment of corner conditions

For the second term in (13), integrating by parts over a smooth segment C of $\partial\Omega$ having corner points C_0 and C_1 yields

$$(\tau_K \partial_K \psi, \tau_J n_I M_{IJ} w)_C = [\psi \tau_J n_I M_{IJ} w]_{C_0}^{C_1} - (\psi, \tau_K \partial_K \tau_J n_I M_{IJ} w)_C.$$
(14)

Note that whenever we have a normal (or a tangent) that has two different directions at a given point when approached from opposite directions along the boundary, that point is considered a corner. Combining all boundary terms, (11) becomes

$$BT = (\psi, n_J \partial_I M_{IJ} w + \tau_K \partial_K \tau_J n_I M_{IJ} w)_{\partial\Omega} - (n_I \partial_I \psi, n_J n_I M_{IJ} w)_{\partial\Omega} - \sum_{\alpha} [\psi \tau_J n_I M_{IJ} w]_{C_0^{\alpha}}^{C_1^{\alpha}}.$$
(15)

Notation is further simplified by defining the normal bending moment operator,

$$M_{nn} = n_I n_I M_{IJ}, \tag{16}$$

tangential bending moment operator,

$$M_{\tau n} = \tau_I n_I M_{IJ},\tag{17}$$

and shear force operator,

$$V_n = n_J \partial_I M_{IJ} + \tau_I \partial_I M_{\tau n}. \tag{18}$$

With this notation, we write the weak form as

$$(m\psi, \ddot{w})_{\Omega} + (\partial_I \partial_J \psi, -M_{IJ} w)_{\Omega} = (\psi, V_n w)_{\partial\Omega} - (n_I \partial_I \psi, M_{nn} w)_{\partial\Omega} - \sum_{\alpha} [\psi M_{\tau n} w]_{C_0^{\alpha}}^{C_0^{\alpha}}. \quad (19)$$

Finally, the mechanical energy balance is obtained by setting $\psi = \dot{w}$ in (19):

$$(m\dot{w}, \ddot{w})_{\Omega} + (\partial_I \partial_J \dot{w}, -M_{IJ} w)_{\Omega} = (\dot{w}, V_n w)_{\partial \Omega} - (n_I \partial_I \dot{w}, M_{nn} w)_{\partial \Omega} - \sum_{\alpha} [\dot{w} M_{\tau n} w]_{C_0^{\alpha}}^{C_1^{\alpha}}. \quad (20)$$

We identify the left side of (20) as the rate of change of the mechanical energy of the plate \mathcal{E} , defined as the sum of kinetic energy and elastic strain energy:

$$\mathcal{E} = \frac{1}{2} \left[(\dot{w}, m\dot{w})_{\Omega} + (\partial_I \partial_J w, -M_{IJ} w)_{\Omega} \right]. \tag{21}$$

This follows from

$$(\partial_{I}\partial_{J}\dot{w}, -M_{IJ}w)_{\Omega} = (\partial_{I}\partial_{I}\dot{w}, \nu B\partial_{J}\partial_{J}w)_{\Omega} + (\partial_{I}\partial_{J}\dot{w}, (1-\nu)B\partial_{I}\partial_{J}w)_{\Omega}$$

$$= \frac{1}{2}\frac{d}{dt} \left[(\partial_{I}\partial_{I}w, \nu B\partial_{J}\partial_{J}w)_{\Omega} + (\partial_{I}\partial_{J}w, (1-\nu)B\partial_{I}\partial_{J}w)_{\Omega} \right]$$

$$= \frac{1}{2}\frac{d}{dt} \left[(\partial_{I}\partial_{J}w, \nu B\delta_{IJ}\partial_{K}\partial_{K}w)_{\Omega} + (\partial_{I}\partial_{J}w, (1-\nu)B\partial_{I}\partial_{J}w)_{\Omega} \right]$$

$$= \frac{1}{2}\frac{d}{dt} \left(\partial_{I}\partial_{J}w, -M_{IJ}w \right)_{\Omega}.$$
(22)

Here $(\partial_I \partial_J w, -M_{IJ} w)_{\Omega}$ is non-negative for the typical conditions $0 \le \nu \le 1/2$ and $B \ge 0$ [19]. Thus we write (20) as

$$\frac{\mathrm{d}\mathcal{E}}{\mathrm{d}t} = \mathrm{BT},\tag{23}$$

where the boundary terms correspond to the power, or rate of work, during deformation against the shear force and moments on the boundary and corners:

$$BT = (\dot{w}, V_n w)_{\partial\Omega} - (n_I \partial_I \dot{w}, M_{nn} w)_{\partial\Omega} - \sum_{\alpha} [\dot{w} M_{\tau n} w]_{C_0^{\alpha}}^{C_1^{\alpha}}.$$
 (24)

Standard boundary conditions include homogeneous clamped boundary conditions, [29]

$$w = 0,$$
 $\vec{X} \in \partial\Omega,$ $t \ge 0,$ (25a)

$$n_I \partial_I w = 0,$$
 $\vec{X} \in \partial \Omega,$ $t \ge 0,$ (25b)

as well as free boundary conditions [14] together with corner conditions [17]

$$M_{nn}w = 0,$$
 $\vec{X} \in \partial\Omega,$ $t \ge 0,$ (26a)

$$V_n w = 0,$$
 $\vec{X} \in \partial \Omega,$ $t \ge 0,$ (26b)

$$M_{\tau n}w\Big|_{i}^{\vec{X}=C_{i}^{\alpha}}=0, \qquad \forall \alpha \text{ and } i \in \{0,1\}, \qquad t \geq 0$$
 (26c)

both of which yield energy conservation and are considered of our work. Other boundary and corner conditions are possible [29], and the numerical treatment of these cases can be deduced from the clamped and free boundary condition cases that we examine in this work.

3.2. Coordinate transformation

Let $\{\vec{e_i}\}$ denote an orthogonal basis in \mathbb{R}^2 and let $\vec{x} = x_i \vec{e_i}$. We introduce a smooth oneto-one mapping $X_I = X_I(x_1, x_2)$ from the reference (or computational) domain $\omega = [0, 1]^2$ to the physical domain Ω (see Fig. 2). From here on, we will use uppercase letters for the quantities in the physical domain and lowercase letters for corresponding quantities in the reference domain. Define $\partial_i = \partial/\partial x_i$ and the transformation gradient

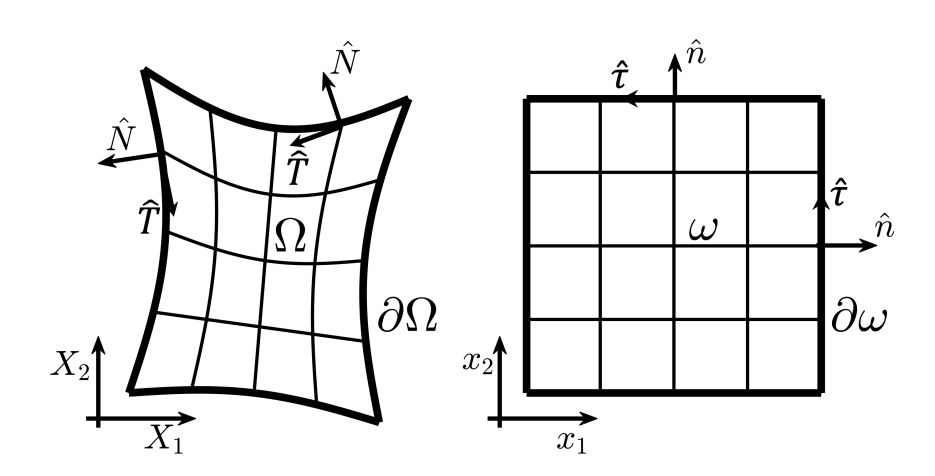


Figure 2: Schematic of the physical domain Ω and the reference domain ω , modified from [2].

by the chain rule,

$$\partial_I = F_{Ii}\partial_i. \tag{27}$$

Further, let

$$J = \det\left[\left(F^{-1} \right)_{iI} \right] \tag{28}$$

be the Jacobian determinant of the mapping from ω to Ω , with J > 0. Recall the following metric identity [35]

$$JF_{Ii}\partial_i = \partial_i JF_{Ii}. (29)$$

The covariant basis vectors \vec{a}_i are

$$\vec{a}_i = \partial_i \vec{X} = \partial_i X_I \vec{E}_I = (F^{-1})_{iI} \vec{E}_I. \tag{30}$$

3.2.1. Integrals and normals

We have $d\Omega = Jd\omega$, since $Jd\omega$ is the area element. Thus,

$$(u,v)_{\Omega} = (u,Jv)_{\omega}. \tag{31}$$

Similarly, we let \hat{J} denote the arc length scale factor so that

$$(u,v)_{\partial\Omega} = \left(u,\hat{J}v\right)_{\partial\omega}.$$
 (32)

In two space dimensions the surface area scale factor \hat{J} is related to the covariant basis vectors \vec{a}_i as follows:

$$\hat{J} = |\vec{a}_i|, \quad x_j \in \{0, 1\}, \quad i, j \text{ cyclic.}$$
 (33)

The normals $\hat{N} = n_I \vec{E}_I$ and $\hat{n} = n_i \vec{e}_i$ are related by Nanson's formula [19],

$$\hat{J}n_I = JF_{Ii}n_i. (34)$$

Similarly, the tangents $\hat{T} = \tau_I \vec{E}_I$ and $\hat{\tau} = \tau_i \vec{e}_i$ satisfy

$$\hat{J}\tau_I = JF_{Ii}\tau_i. \tag{35}$$

3.3. Numerical approximation of the transformation gradient

In this subsection we provide a brief comment on numerical treatment of derivatives involved in the mapping. An approximation $F_{Ii} \approx F_{Ii}$ of the transformation gradient can be computed by applying difference approximations on the same grid used to solve the PDE. When this is done, F_{Ii} must be computed to the same order of accuracy or higher as the difference operators used to discretize the PDEs in order to retain the order of accuracy of overall scheme. For all our numerical experiments in this paper, we compute F_{Ii} using the first-derivative SBP operators of the same order as we use to solve the PDEs, which means that F_{Ii} is computed to order q and q near boundaries and in the interior, respectively.

Note that Nanson's formula (34) is identical for approximated quantities, because we used Nanson's formula to define \hat{n} . As long as the resulting Jacobian determinant is positive, we conclude that F_{Ii} can be computed with any sufficiently accurate method. Thus, with a bit of notation abuse, we drop the underline notation and use the non-underline notation interchangeably between continuous and discrete settings, as in [1].

4. Summation-by-parts operators

The notations in this section closely follow [2]. Only diagonal-norm SBP operators are considered here. Hence, the norm matrix P_x has the following structure

$$P_{\mathcal{X}} = \operatorname{diag}(p_1, p_2, \dots, p_2, p_1),$$
 (36)

where p_i , $\forall i$ are proportional to the grid spacing Δx in the reference domain. Define $D_{\mathcal{X}} \approx \partial_{\mathcal{X}}$ as a first-derivative SBP operator. It has the SBP property

$$P_{\mathcal{X}}D_{\mathcal{X}} = -D_{\mathcal{X}}^{T}P_{\mathcal{X}} - e_{0}e_{0}^{T} + e_{N}e_{N}^{T}, \tag{37}$$

where

$$e_0 = \begin{bmatrix} 1 & 0 & \dots & 0 \end{bmatrix}^T, \quad e_N = \begin{bmatrix} 0 & \dots & 0 & 1 \end{bmatrix}^T.$$
 (38)

4.1. Two-dimensional first-derivative operators

As in [2], let operators with subscripts \mathcal{X}_i denote one-dimensional operators which correspond to coordinate direction \mathcal{X}_i . The multidimensional first derivatives $D_i \approx \partial_i$ are constructed using tensor products:

$$D_i = I_{\mathcal{X}_1} \otimes D_{\mathcal{X}_i} \text{ or } D_i = D_{\mathcal{X}_i} \otimes I_{\mathcal{X}_d}, \tag{39}$$

where $I_{\mathcal{X}_i}$, $\forall i$ are one-dimensional identity matrices of appropriate sizes. In analogy with the chain rule (27) and the metric identities, we define

$$\partial_I \approx D_I = F_{Ii} D_i \tag{40}$$

and

$$\partial_I \approx \widetilde{D}_I = J^{-1} D_i J F_{Ii}. \tag{41}$$

In the discrete setting, F_{Ii} should be interpreted as a diagonal matrix with the grid point values of the continuous F_{Ii} for each fixed indices of I and i. Similarly, D_i is a matrix for each fixed i. Thus, the implied summation in $F_{Ii}D_i$ is an addition operator in $\mathbb{R}^{N\times N}$, where N denotes total number of grid points.

We also define two-dimensional normal and tangential first derivative operators on reference

$$D_n = n_i D_i, \quad D_\tau = \tau_i D_i \tag{42}$$

and on physical

$$D_N = n_I D_I, \quad D_T = \tau_I D_I \tag{43}$$

domains. Now using the fact that

$$\delta_{IJ} = n_I n_J + \tau_I \tau_J, \tag{44}$$

we can state the following

$$D_I = n_I n_J D_J + \tau_I \tau_J D_J = n_I D_N + \tau_I D_T, \tag{45}$$

which is a discrete equivalent of (12). The two-dimensional quadrature is

$$P = P_{\mathcal{X}_1} \otimes P_{\mathcal{X}_d},\tag{46}$$

and we define

$$(\mathbf{u}, \mathbf{v})_{\omega} = \mathbf{u}^T P \mathbf{v} \tag{47}$$

for discrete integration over the reference domain ω . Next, for integration over boundary faces, denote $\partial \omega_i^-$ and $\partial \omega_i^+$ to be the boundary faces where $x_i = 0$ and $x_i = 1$, respectively. Now define

$$P_{\partial \omega_i} = P_{\mathcal{X}_1} \otimes \cdots \otimes P_{\mathcal{X}_{i-1}} \otimes P_{\mathcal{X}_{i+1}} \otimes \cdots \otimes P_{\mathcal{X}_d}. \tag{48}$$

 $P_{\partial\omega_i}$ could be used to integrate over both $\partial\omega_i^+$ and $\partial\omega_i^-$. The same inner product notation is used as in the continuous case, without risk of confusion because the boldface font denotes discrete solution vectors.

Let e_f^T be a restriction operator that selects only those solution values that reside on the face f. For integration over f, we write

$$(\mathbf{u}, \mathbf{v})_f = (e_f^T \mathbf{u})^T P_f (e_f^T \mathbf{v}). \tag{49}$$

For integration over the entire boundary $\partial \omega$ we define

$$(\mathbf{u}, \mathbf{v})_{\partial\omega} = \sum_{f \subset \partial\omega} (\mathbf{u}, \mathbf{v})_f.$$
 (50)

This means that the integration is performed over one face at a time. Similarly as in (31) and (32), let us define

$$(\mathbf{u}, \mathbf{v})_{\Omega} = (\mathbf{u}, J\mathbf{v})_{\omega} \tag{51}$$

and

$$(\mathbf{u}, \mathbf{v})_{\partial\Omega} = (\mathbf{u}, \hat{J}\mathbf{v})_{\partial\Omega}.$$
 (52)

With the above notations, we have the summation-by-parts formula

$$(\mathbf{u}, D_i \mathbf{v})_{\omega} = (\mathbf{u}, n_i \mathbf{v})_{\partial \omega} - (D_i \mathbf{u}, \mathbf{v})_{\omega}.$$
(53)

Let us establish a relation between D_I and \widetilde{D}_I .

Lemma 1. D_I and \widetilde{D}_I have the following summation-by-parts property:

$$\left(\mathbf{u}, \widetilde{D}_I \mathbf{v}\right)_{\Omega} = \left(\mathbf{u}, n_I \mathbf{v}\right)_{\partial \Omega} - \left(D_I \mathbf{u}, \mathbf{v}\right)_{\Omega}.$$
 (54)

Proof.

$$\begin{pmatrix} \mathbf{u}, \widetilde{D}_{I} \mathbf{v} \end{pmatrix}_{\Omega} = \begin{pmatrix} \mathbf{u}, J^{-1} D_{i} J F_{Ii} \mathbf{v} \end{pmatrix}_{\Omega} = \begin{pmatrix} \mathbf{u}, J J^{-1} D_{i} J F_{Ii} \mathbf{v} \end{pmatrix}_{\omega}
= \begin{pmatrix} \mathbf{u}, D_{i} J F_{Ii} \mathbf{v} \end{pmatrix}_{\omega} \qquad (\text{use } (53))
= \begin{pmatrix} \mathbf{u}, n_{i} J F_{Ii} \mathbf{v} \end{pmatrix}_{\partial \omega} - \begin{pmatrix} D_{i} \mathbf{u}, J F_{Ii} \mathbf{v} \end{pmatrix}_{\omega} \qquad (\text{use } (34))
= \begin{pmatrix} \mathbf{u}, \widehat{J} n_{I} \mathbf{v} \end{pmatrix}_{\partial \omega} - \begin{pmatrix} D_{i} \mathbf{u}, J F_{Ii} \mathbf{v} \end{pmatrix}_{\omega}
= \begin{pmatrix} \mathbf{u}, \widehat{J} n_{I} \mathbf{v} \end{pmatrix}_{\partial \omega} - \begin{pmatrix} F_{Ii} D_{i} \mathbf{u}, J \mathbf{v} \end{pmatrix}_{\omega}
= \begin{pmatrix} \mathbf{u}, n_{I} \mathbf{v} \end{pmatrix}_{\partial \Omega} - \begin{pmatrix} D_{I} \mathbf{u}, J \mathbf{v} \end{pmatrix}_{\omega}
= \begin{pmatrix} \mathbf{u}, n_{I} \mathbf{v} \end{pmatrix}_{\partial \Omega} - \begin{pmatrix} D_{I} \mathbf{u}, J \mathbf{v} \end{pmatrix}_{\Omega}.$$

Finally, let us introduce a summation-by-parts formula in a boundary integral involving the tangential derivatives:

$$(\mathbf{u}, D_T \mathbf{v})_{\partial\Omega} = (\mathbf{u}, \hat{J} D_T)_{\partial\omega} = (\mathbf{u}, D_t \mathbf{v})_{\partial\omega} = \sum_{\alpha} \mathbf{u}^T \left(\mathbf{v} \Big|_{C_0^{\alpha}}^{C_1^{\alpha}} \right) - (D_t \mathbf{u}, \mathbf{v})_{\partial\omega}$$

$$= \sum_{\alpha} \mathbf{u}^T \left(\mathbf{v} \Big|_{C_0^{\alpha}}^{C_1^{\alpha}} \right) - (D_T \mathbf{u}, \mathbf{v})_{\partial\Omega},$$
(55)

where $\mathbf{v}\Big|_{C_0^{\alpha}}^{C^{\alpha}}$ is a zero vector with non-zero values $-v(C_0^{\alpha})$ and $v(C_1^{\alpha})$ at the corner points C_0^{α} and C_1^{α} , respectively.

5. Multiblock SBP operators

The above concepts and notations can be extended to multiple grid blocks coupled across internal interfaces, across which the Jacobian J and the transformation gradient F_{Ii} may be discontinuous. We restrict attention to conforming meshes having collocated grid points on the two sides of the interface.

Let Γ denote the interface between two domains Ω_u and Ω_v , and let $\Omega = \Omega_u \cup \Omega_v$. Let

$$\mathbf{w} = \begin{bmatrix} \mathbf{u} \\ \mathbf{v} \end{bmatrix}, \quad \boldsymbol{\psi} = \begin{bmatrix} \boldsymbol{\phi} \\ \boldsymbol{\chi} \end{bmatrix}, \tag{56}$$

denote grid functions with the top and bottom blocks corresponding to Ω_u and Ω_v , respectively. Define the two-block operators

$$\mathbb{D}_{I}\mathbf{w} = \begin{bmatrix} D_{I}^{u}\mathbf{u} - \frac{1}{2} (J^{u}P^{u})^{-1} e_{\Gamma}^{u} n_{I}^{u} \hat{J} P_{\Gamma} \left((e_{\Gamma}^{u})^{T} \mathbf{u} - (e_{\Gamma}^{v})^{T} \mathbf{v} \right) \\ D_{I}^{v}\mathbf{v} - \frac{1}{2} (J^{v}P^{v})^{-1} e_{\Gamma}^{v} n_{I}^{v} \hat{J} P_{\Gamma} \left((e_{\Gamma}^{v})^{T} \mathbf{v} - (e_{\Gamma}^{u})^{T} \mathbf{u} \right) \end{bmatrix}$$

$$(57)$$

and

$$\widetilde{\mathbb{D}}_{I}\mathbf{w} = \begin{bmatrix} \widetilde{D}_{I}^{u}\mathbf{u} - \frac{1}{2}(J^{u}P^{u})^{-1}e_{\Gamma}^{u}n_{I}^{u}\widehat{J}P_{\Gamma}\left(\left(e_{\Gamma}^{u}\right)^{T}\mathbf{u} - \left(e_{\Gamma}^{v}\right)^{T}\mathbf{v}\right) \\ \widetilde{D}_{I}^{v}\mathbf{v} - \frac{1}{2}(J^{v}P^{v})^{-1}e_{\Gamma}^{v}n_{I}^{v}\widehat{J}P_{\Gamma}\left(\left(e_{\Gamma}^{v}\right)^{T}\mathbf{v} - \left(e_{\Gamma}^{u}\right)^{T}\mathbf{u}\right) \end{bmatrix}$$
(58)

If w is continuous across Γ , then $\mathbb{D}_I \mathbf{w}$ is a consistent approximation of $\partial_I w$ in all of Ω . If, additionally, $\partial_I w$ is continuous across Γ , then $\mathbb{D}_I \mathbf{w}$ is continuous to the order of accuracy of the underlying finite difference operators. The same is true for $\widetilde{\mathbb{D}}_I \mathbf{w}$.

Lemma 2. The multi-block operators \mathbb{D}_I and $\widetilde{\mathbb{D}}_I$ satisfy the following summation-by-parts formula on the multi-block domain Ω .

$$(\boldsymbol{\psi}, \mathbb{D}_I \mathbf{w})_{\Omega} = (\boldsymbol{\psi}, n_I \mathbf{w})_{\partial \Omega} - (\boldsymbol{\psi}, \widetilde{\mathbb{D}}_I \mathbf{w})_{\Omega}.$$
 (59)

Proof. The proof is shown for two blocks, but can immediately be extended to arbitrarily many blocks. By the definitions of \mathbb{D}_I and $\widetilde{\mathbb{D}}_I$, we have

$$(\boldsymbol{\psi}, \mathbb{D}_{I}\mathbf{w})_{\Omega} = (\boldsymbol{\phi}, D_{I}^{u}\mathbf{u})_{\Omega_{u}} - \frac{1}{2} (n_{I}^{u}\boldsymbol{\phi}, \mathbf{u} - \mathbf{v})_{\Gamma} + (\boldsymbol{\chi}, D_{I}^{v}\mathbf{v})_{\Omega_{v}} - \frac{1}{2} (n_{I}^{v}\boldsymbol{\chi}, \mathbf{v} - \mathbf{u})_{\Gamma}$$
(60)

and

$$\left(\widetilde{\mathbb{D}}_{I}\boldsymbol{\psi},\mathbf{w}\right)_{\Omega} = \left(\widetilde{D}_{I}^{u}\boldsymbol{\phi},\mathbf{u}\right)_{\Omega_{u}} - \frac{1}{2}\left(n_{I}^{u}\mathbf{u},\boldsymbol{\phi}-\boldsymbol{\chi}\right)_{\Gamma} + \left(\widetilde{D}_{I}^{v}\boldsymbol{\chi},\mathbf{v}\right)_{\Omega_{v}} - \frac{1}{2}\left(n_{I}^{v}\mathbf{v},\boldsymbol{\chi}-\boldsymbol{\phi}\right)_{\Gamma}.$$
 (61)

Using the SBP properties of the single-block operators (54) $D_I^{u,v}$ yields

$$(\boldsymbol{\psi}, \mathbb{D}_{I}\mathbf{w})_{\Omega} = -\left(\widetilde{D}_{I}^{u}\boldsymbol{\phi}, \mathbf{u}\right)_{\Omega_{u}} + (n_{I}^{u}\boldsymbol{\phi}, \mathbf{u})_{\Gamma_{u}} + (n_{I}^{u}\boldsymbol{\phi}, \mathbf{u})_{\Gamma} - \frac{1}{2}(n_{I}^{u}\boldsymbol{\phi}, \mathbf{u} - \mathbf{v})_{\Gamma} - \left(\widetilde{D}_{I}^{v}\boldsymbol{\chi}, \mathbf{v}\right)_{\Omega_{v}} + (n_{I}^{v}\boldsymbol{\chi}, \mathbf{v})_{\Gamma_{v}} + (n_{I}^{v}\boldsymbol{\chi}, \mathbf{v})_{\Gamma} - \frac{1}{2}(n_{I}^{v}\boldsymbol{\chi}, \mathbf{v} - \mathbf{u})_{\Gamma},$$

$$(62)$$

where $\Gamma_u = \partial \Omega_u \setminus \Gamma$ and $\Gamma_v = \partial \Omega_v \setminus \Gamma$. The discrete surface integral over $\partial \Omega$ is defined as the sum of the corresponding integrals over Γ_u and Γ_v so that, by definition,

$$(n_I \boldsymbol{\psi}, \mathbf{w})_{\partial\Omega} = (n_I^u \boldsymbol{\phi}, \mathbf{u})_{\Gamma_u} + (n_I^v \boldsymbol{\chi}, \mathbf{v})_{\Gamma_v}.$$
(63)

It follows that

$$(\boldsymbol{\psi}, \mathbb{D}_{I}\mathbf{w})_{\Omega} = (n_{I}\boldsymbol{\psi}, \mathbf{w})_{\partial\Omega} - \left(\widetilde{D}_{I}^{u}\boldsymbol{\phi}, \mathbf{u}\right)_{\Omega_{u}} + (n_{I}^{u}\boldsymbol{\phi}, \mathbf{u})_{\Gamma} - \frac{1}{2}(n_{I}^{u}\boldsymbol{\phi}, \mathbf{u} - \mathbf{v})_{\Gamma} - \left(\widetilde{D}_{I}^{v}\boldsymbol{\chi}, \mathbf{v}\right)_{\Omega_{v}} + (n_{I}^{v}\boldsymbol{\chi}, \mathbf{v})_{\Gamma} - \frac{1}{2}(n_{I}^{v}\boldsymbol{\chi}, \mathbf{v} - \mathbf{u})_{\Gamma}$$

$$= (n_{I}\boldsymbol{\psi}, \mathbf{w})_{\partial\Omega} - \left(\widetilde{D}_{I}^{u}\boldsymbol{\phi}, \mathbf{u}\right)_{\Omega_{u}} + \frac{1}{2}(\mathbf{u}, n_{I}^{u}\boldsymbol{\phi} + n_{I}^{v}\boldsymbol{\chi})_{\Gamma} - \left(\widetilde{D}_{I}^{v}\boldsymbol{\chi}, \mathbf{v}\right)_{\Omega_{v}} + \frac{1}{2}(\mathbf{v}, n_{I}^{v}\boldsymbol{\chi} + n_{I}^{u}\boldsymbol{\phi})_{\Gamma}.$$

$$(64)$$

We compute the numerical approximation of the transformation gradient so that $n_I^u = -n_I^v$ holds exactly in the discrete setting. Using this, we obtain

$$(\boldsymbol{\psi}, \mathbb{D}_{I}\mathbf{w})_{\Omega} = (n_{I}\boldsymbol{\psi}, \mathbf{w})_{\partial\Omega} - \left(\widetilde{D}_{I}^{u}\boldsymbol{\phi}, \mathbf{u}\right)_{\Omega_{u}} + \frac{1}{2}\left(n_{I}^{u}\mathbf{u}, \boldsymbol{\phi} - \boldsymbol{\chi}\right)_{\Gamma} - \left(\widetilde{D}_{I}^{v}\boldsymbol{\chi}, \mathbf{v}\right)_{\Omega_{v}} + \frac{1}{2}\left(n_{I}^{v}\mathbf{v}, \boldsymbol{\chi} - \boldsymbol{\phi}\right)_{\Gamma}$$

$$= (n_{I}\boldsymbol{\psi}, \mathbf{w})_{\partial\Omega} - \left(\widetilde{\mathbb{D}}_{I}\boldsymbol{\psi}, \mathbf{w}\right)_{\Omega}.$$

$$(65)$$

From now on, we will use blackboard bold typeface, e.g. \mathbb{D} , to define discrete differential operators.

5.1. The discrete plate operator

We define the following discrete versions of plate, moment, normal bending moment, tangential bending moment, and shear force operators as

$$\mathbb{D}_4 = -\mathbb{D}_2 \nu B \mathbb{D}_2 - \widetilde{\mathbb{D}}_J \widetilde{\mathbb{D}}_I (1 - \nu) B \mathbb{D}_I \mathbb{D}_J, \tag{66}$$

$$\mathbb{M}_{IJ} = -\nu B \delta_{IJ} \mathbb{D}_2 - (1 - \nu) B \mathbb{D}_I \mathbb{D}_J, \tag{67}$$

$$\mathbb{M}_{nn} = n_J n_I \mathbb{M}_{IJ},\tag{68}$$

$$\mathbb{M}_{\tau n} = \tau_J n_I \mathbb{M}_{IJ} \tag{69}$$

and

$$V_n = -n_J \mathbb{D}_I \nu B \delta_{IJ} \mathbb{D}_2 - n_J \widetilde{\mathbb{D}}_I (1 - \nu) B \mathbb{D}_I \mathbb{D}_J + \mathbb{D}_T \tau_I n_I \mathbb{M}_{IJ}, \tag{70}$$

respectively. The second-derivatives $\partial_I \partial_I$ can be approximated using both wide, $\mathbb{D}_I \mathbb{D}_I$, and narrow-stencil, \mathbb{D}_2 , operators. We use the narrow-stencil second-derivative operator because it is more accurate and robust than the wide-stencil approximations [21].

In order to obtain summation-by-parts formulas for the physical domain, let us restate the formula from equation (110) from [2]:

$$(\mathbf{u}, \mathbb{D}_2 \mathbf{v})_{\Omega} = (\mathbf{u}, n_I \mathbb{D}_I \mathbf{v})_{\partial \Omega} - (n_I \mathbb{D}_I \mathbf{u}, \mathbf{v})_{\partial \Omega} + (\mathbb{D}_2 \mathbf{u}, \mathbf{v})_{\Omega},$$
(71)

where \mathbb{D}_2 is a narrow-stencil SBP operator for $\partial_I \partial_I$. Now we can construct a finite difference operator that approximates the plate operator $\partial_J \partial_I M_{IJ}$ on the physical domain. First, let us rewrite $\partial_J \partial_I M_{IJ}$

$$\partial_J \partial_I M_{IJ} = -\partial_J \partial_J \nu B \partial_I \partial_I - \partial_J \partial_I (1 - \nu) B \partial_I \partial_J. \tag{72}$$

Theorem 3. The discrete plate operator \mathbb{D}_4 satisfies the summation-by-parts formula

$$(\mathbf{u}, \mathbb{D}_{4}\mathbf{v})_{\Omega} = -(\mathbb{D}_{2}\mathbf{u}, \nu B \mathbb{D}_{2}\mathbf{v})_{\Omega} - (\mathbb{D}_{I}\mathbb{D}_{J}\mathbf{u}, (1-\nu)B\mathbb{D}_{I}\mathbb{D}_{J}\mathbf{v})_{\Omega} + (\mathbf{u}, \mathbb{V}_{n}\mathbf{v})_{\partial\Omega} - (\mathbb{D}_{N}\mathbf{u}, \mathbb{M}_{nn}\mathbf{v})_{\partial\Omega} - \sum_{\alpha} \mathbf{u}^{T} \left(\mathbb{M}_{\tau n}\mathbf{v} \Big|_{C_{0}^{\alpha}}^{C_{1}^{\alpha}} \right).$$

$$(73)$$

Proof. First, using (71), we obtain

$$(\mathbf{u}, \mathbb{D}_2 \nu B \mathbb{D}_2 \mathbf{v})_{\Omega} = (\mathbb{D}_2 \mathbf{u}, \nu B \mathbb{D}_2 \mathbf{v})_{\Omega} + (\mathbf{u}, n_I \mathbb{D}_I \nu B \mathbb{D}_2 \mathbf{v})_{\partial \Omega} - (n_I \mathbb{D}_I \mathbf{u}, \nu B \mathbb{D}_2 \mathbf{v})_{\partial \Omega}. \tag{74}$$

Second, we have

$$\left(\mathbf{u}, \widetilde{\mathbb{D}}_{J}\widetilde{\mathbb{D}}_{I}(1-\nu)B\mathbb{D}_{I}\mathbb{D}_{J}\mathbf{v}\right)_{\Omega} \qquad (\text{use } (59))$$

$$= \left(\mathbf{u}, n_{J}\widetilde{\mathbb{D}}_{I}(1-\nu)B\mathbb{D}_{I}\mathbb{D}_{J}\mathbf{v}\right)_{\partial\Omega} - \left(\mathbb{D}_{J}\mathbf{u}, \widetilde{\mathbb{D}}_{I}(1-\nu)B\mathbb{D}_{I}\mathbb{D}_{J}\mathbf{v}\right)_{\Omega} \qquad (\text{use } (59))$$

$$= \left(\mathbb{D}_{I}\mathbb{D}_{J}\mathbf{u}, (1-\nu)B\mathbb{D}_{I}\mathbb{D}_{J}\mathbf{v}\right)_{\Omega} + \left(\mathbf{u}, n_{J}\widetilde{\mathbb{D}}_{I}(1-\nu)B\mathbb{D}_{I}\mathbb{D}_{J}\mathbf{v}\right)_{\partial\Omega}$$

$$- \left(\mathbb{D}_{J}\mathbf{u}, n_{I}(1-\nu)B\mathbb{D}_{I}\mathbb{D}_{J}\mathbf{v}\right)_{\partial\Omega}.$$
(15)

Let us focus on the last term. Now using (45), we have

$$(\mathbb{D}_{J}\mathbf{u}, n_{I}(1-\nu)B\mathbb{D}_{I}\mathbb{D}_{J}\mathbf{v})_{\partial\Omega} = ([n_{J}\mathbb{D}_{N} + \tau_{J}\mathbb{D}_{T}]\mathbf{u}, n_{I}(1-\nu)B\mathbb{D}_{I}\mathbb{D}_{J}\mathbf{v})_{\partial\Omega}$$

$$= (\mathbb{D}_{N}\mathbf{u}, n_{J}n_{I}(1-\nu)B\mathbb{D}_{I}\mathbb{D}_{J}\mathbf{v})_{\partial\Omega} + (\tau_{J}\mathbb{D}_{T}\mathbf{u}, n_{I}(1-\nu)B\mathbb{D}_{I}\mathbb{D}_{J}\mathbf{v})_{\partial\Omega}$$

$$= (\mathbb{D}_{N}\mathbf{u}, n_{J}n_{I}(1-\nu)B\mathbb{D}_{I}\mathbb{D}_{J}\mathbf{v})_{\partial\Omega} + (\mathbb{D}_{T}\mathbf{u}, \tau_{J}n_{I}(1-\nu)B\mathbb{D}_{I}\mathbb{D}_{J}\mathbf{v})_{\partial\Omega}$$

$$= (\mathbb{D}_{N}\mathbf{u}, n_{J}n_{I}(1-\nu)B\mathbb{D}_{I}\mathbb{D}_{J}\mathbf{v})_{\partial\Omega} - (\mathbf{u}, \mathbb{D}_{T}\tau_{J}n_{I}(1-\nu)B\mathbb{D}_{I}\mathbb{D}_{J}\mathbf{v})_{\partial\Omega}$$

$$+ \sum_{\alpha} \mathbf{u}^{T} \left(\tau_{J}n_{I}(1-\nu)B\mathbb{D}_{I}\mathbb{D}_{J}\mathbf{v}\Big|_{C_{0}^{\alpha}}^{C_{1}^{\alpha}}\right).$$

$$(76)$$

Knowing that $\tau_I n_I = 0$ and $n_I n_I = 1$, we rewrite operators (68), (69), and (70) as

$$\mathbb{M}_{nn} = n_J n_I \mathbb{M}_{IJ} = -n_J n_I \nu B \delta_{IJ} \mathbb{D}_2 - n_J n_I (1 - \nu) B \mathbb{D}_I \mathbb{D}_J = -\nu B \mathbb{D}_2 - n_J n_I (1 - \nu) B \mathbb{D}_I \mathbb{D}_J,$$
(77)

$$\mathbb{M}_{\tau n} = \tau_J n_I \mathbb{M}_{IJ} = -\tau_J n_I \nu B \delta_{IJ} \mathbb{D}_2 - \tau_J n_I (1 - \nu) B \mathbb{D}_I \mathbb{D}_J = -\tau_J n_I (1 - \nu) B \mathbb{D}_I \mathbb{D}_J, \quad (78)$$
and

$$\mathbb{V}_{n} = -n_{J} \mathbb{D}_{I} \nu B \delta_{IJ} \mathbb{D}_{2} - n_{J} \widetilde{\mathbb{D}}_{I} (1 - \nu) B \mathbb{D}_{I} \mathbb{D}_{J} + \mathbb{D}_{T} \tau_{J} n_{I} \mathbb{M}_{IJ}
= -n_{I} \mathbb{D}_{I} \nu B \mathbb{D}_{2} - n_{J} \widetilde{\mathbb{D}}_{I} (1 - \nu) B \mathbb{D}_{I} \mathbb{D}_{J} - \mathbb{D}_{T} \tau_{J} n_{I} \nu B \delta_{IJ} \mathbb{D}_{2} - \mathbb{D}_{T} \tau_{J} n_{I} (1 - \nu) B \mathbb{D}_{I} \mathbb{D}_{J} \quad (79)
= -n_{I} \mathbb{D}_{I} \nu B \mathbb{D}_{2} - n_{J} \widetilde{\mathbb{D}}_{I} (1 - \nu) B \mathbb{D}_{I} \mathbb{D}_{J} - \mathbb{D}_{T} \tau_{J} n_{I} (1 - \nu) B \mathbb{D}_{I} \mathbb{D}_{J},$$

respectively. Finally, substituting (76) into (75) and adding (75) to (74) and using equations

(77), (78), and (79), we obtain

$$(\mathbf{u}, \mathbb{D}_{4}\mathbf{v})_{\Omega}$$

$$= -(\mathbb{D}_{2}\mathbf{u}, \nu B \mathbb{D}_{2}\mathbf{v})_{\Omega} - (\mathbb{D}_{I}\mathbb{D}_{J}\mathbf{u}, (1 - \nu)B\mathbb{D}_{I}\mathbb{D}_{J}\mathbf{v})_{\Omega}$$

$$+ (\mathbb{D}_{N}\mathbf{u}, \nu B \mathbb{D}_{2}\mathbf{v})_{\partial\Omega} + (\mathbb{D}_{N}\mathbf{u}, n_{J}n_{I}(1 - \nu)B\mathbb{D}_{I}\mathbb{D}_{J}\mathbf{v})_{\partial\Omega}$$

$$- (\mathbf{u}, n_{I}\mathbb{D}_{I}\nu B \mathbb{D}_{2}\mathbf{v})_{\partial\Omega} - (\mathbf{u}, n_{J}\widetilde{\mathbb{D}}_{I}(1 - \nu)B\mathbb{D}_{I}\mathbb{D}_{J}\mathbf{v})_{\partial\Omega} - (\mathbf{u}, \mathbb{D}_{T}\tau_{J}n_{I}(1 - \nu)B\mathbb{D}_{I}\mathbb{D}_{J}\mathbf{v})_{\partial\Omega}$$

$$+ \sum_{\alpha} \mathbf{u}^{T} \left(\tau_{J}n_{I}(1 - \nu)B\mathbb{D}_{I}\mathbb{D}_{J}\mathbf{v} \Big|_{C_{0}^{\alpha}}^{C_{1}^{\alpha}} \right)$$

$$= -(\mathbb{D}_{2}\mathbf{u}, \nu B \mathbb{D}_{2}\mathbf{v})_{\Omega} - (\mathbb{D}_{I}\mathbb{D}_{J}\mathbf{u}, (1 - \nu)B\mathbb{D}_{I}\mathbb{D}_{J}\mathbf{v})_{\Omega}$$

$$-(\mathbb{D}_{N}\mathbf{u}, \mathbb{M}_{nn}\mathbf{v})_{\partial\Omega} + (\mathbf{u}, \mathbb{V}_{n}\mathbf{v})_{\partial\Omega} - \sum_{\alpha} \mathbf{u}^{T} \left(\mathbb{M}_{\tau n}\mathbf{v} \Big|_{C_{0}^{\alpha}}^{C_{1}^{\alpha}} \right).$$

6. Energy-stable and self-adjoint boundary SATs for the multiblock plate operator

We discretize (7a) in space as

$$m\ddot{\mathbf{w}} = \mathbb{D}_4 \mathbf{w} + SAT, \tag{80}$$

where the SATs in SAT enforce the boundary conditions and will be derived later. Given an arbitrary test function ϕ , we obtain the semi-discrete weak form by multiplying (80) by $\phi^T JP$,

$$(\boldsymbol{\phi}, m\ddot{\mathbf{w}})_{\Omega} = (\boldsymbol{\phi}, \mathbb{D}_4 \mathbf{w})_{\Omega} + (\boldsymbol{\phi}, SAT)_{\Omega},$$
 (81)

and using summation-by-parts (73), we get

$$(\boldsymbol{\phi}, m\ddot{\mathbf{w}})_{\Omega} = -\left(\mathbb{D}_{2}\boldsymbol{\phi}, \nu B \mathbb{D}_{2}\mathbf{w}\right)_{\Omega} - \left(\mathbb{D}_{I}\mathbb{D}_{J}\boldsymbol{\phi}, (1-\nu)B\mathbb{D}_{I}\mathbb{D}_{J}\mathbf{w}\right)_{\Omega} - \left(\mathbb{D}_{N}\boldsymbol{\phi}, \mathbb{M}_{nn}\mathbf{w}\right)_{\partial\Omega} + \left(\boldsymbol{\phi}, \mathbb{V}_{n}\mathbf{w}\right)_{\partial\Omega} - \sum_{\Omega} \boldsymbol{\phi}^{T} \left(\mathbb{M}_{\tau n}\mathbf{w}\Big|_{C_{0}^{\alpha}}^{C_{1}^{\alpha}}\right) + \left(\boldsymbol{\phi}, SAT\right)_{\Omega}.$$
(82)

Define the inner product

$$M\left(\boldsymbol{\phi}, \mathbf{w}\right) = \left(\boldsymbol{\phi}, m\mathbf{w}\right)_{\Omega},\tag{83}$$

the symmetric positive semidefinite bilinear form

$$K(\boldsymbol{\phi}, \mathbf{w}) = (\mathbb{D}_2 \boldsymbol{\phi}, \nu B \mathbb{D}_2 \mathbf{w})_{\Omega} + (\mathbb{D}_I \mathbb{D}_J \boldsymbol{\phi}, (1 - \nu) B \mathbb{D}_I \mathbb{D}_J \mathbf{w})_{\Omega}, \tag{84}$$

and boundary terms

$$B_1(\boldsymbol{\phi}, \mathbf{w}) = -\left(\mathbb{D}_N \boldsymbol{\phi}, \mathbb{M}_{nn} \mathbf{w}\right)_{\partial \Omega} + \left(\boldsymbol{\phi}, SAT_1\right)_{\Omega}, \tag{85}$$

15

and

$$B_{2}\left(\boldsymbol{\phi}, \mathbf{w}\right) = \left(\boldsymbol{\phi}, \mathbb{V}_{n} \mathbf{w}\right)_{\partial \Omega} - \sum_{\alpha} \boldsymbol{\phi}^{T} \left(\mathbb{M}_{\tau n} \mathbf{w} \Big|_{C_{0}^{\alpha}}^{C_{1}^{\alpha}}\right) + \left(\boldsymbol{\phi}, SAT_{2}\right)_{\Omega}, \tag{86}$$

where $SAT = SAT_1 + SAT_2$. For free boundaries, the SAT_1 penalty will enforce the normal moment boundary condition and the SAT_2 penalty will enforce the shear force boundary condition and corner conditions. For clamped boundaries, SAT_1 will enforce the boundary condition on $n_I \partial_I w$ and the SAT_2 penalty will enforce the boundary condition on w. Finally, by adding we obtain

$$B(\boldsymbol{\phi}, \mathbf{w}) = B_1(\boldsymbol{\phi}, \mathbf{w}) + B_2(\boldsymbol{\phi}, \mathbf{w}). \tag{87}$$

Now we can rewrite the weak form as the following

$$M(\boldsymbol{\phi}, \ddot{\mathbf{w}}) + K(\boldsymbol{\phi}, \mathbf{w}) = B(\boldsymbol{\phi}, \mathbf{w}). \tag{88}$$

We define the semi-discrete total energy

$$E = \frac{1}{2} (\dot{\mathbf{w}}, m\dot{\mathbf{w}})_{\Omega} + \frac{1}{2} (\mathbb{D}_{2}\mathbf{w}, \nu B \mathbb{D}_{2}\mathbf{w})_{\Omega} + \frac{1}{2} (\mathbb{D}_{I}\mathbb{D}_{J}\mathbf{w}, (1 - \nu)B \mathbb{D}_{I}\mathbb{D}_{J}\mathbf{w})_{\Omega}$$
$$= \frac{1}{2} M (\dot{\mathbf{w}}, \dot{\mathbf{w}}) + \frac{1}{2} K (\mathbf{w}, \mathbf{w}).$$
(89)

From above, we conclude that the discrete energy E approximates the continuous energy \mathcal{E} as defined in (21). E is a non-negative quantity, which follows from the non-negativity of M and K. Setting $\phi = \dot{\mathbf{w}}$ in (88) yields the semi-discrete energy balance

$$\frac{\mathrm{d}E}{\mathrm{d}t} = B(\dot{\mathbf{w}}, \mathbf{w}). \tag{90}$$

Next we discuss the selection of the SAT terms. The general strategy is to select the SAT terms to provide a consistent approximation of the boundary and corner conditions, while also requiring that $B(\psi, \mathbf{w}) = 0$ for homogeneous conditions.

6.1. Free boundary and corner conditions

Consider free boundary conditions,

$$M_{nn}w = g,$$
 $\vec{X} \in \partial\Omega,$ $t \ge 0,$ (91)

$$V_n w = h,$$
 $\vec{X} \in \partial \Omega,$ $t \ge 0$ (92)

and corner conditions on surfaces with free boundary conditions,

$$M_{\tau n}w\Big|_{i}^{\vec{X}=C_i^{\alpha}} = l_{C_i^{\alpha}}, \qquad \forall \alpha \text{ and } i \in \{0,1\}, \qquad t \ge 0.$$
 (93)

To enforce (91), we select $SAT_1 = SAT_{d2}$, where SAT_{d2} satisfies

$$(\boldsymbol{\phi}, SAT_{d2})_{\Omega} = (\mathbb{D}_N \boldsymbol{\phi}, \mathbb{M}_{nn} \mathbf{w} - \mathbf{g})_{\partial\Omega}.$$
 (94)

Then, for g = 0, we get

$$B_1(\boldsymbol{\phi}, \mathbf{w}) = -\left(\mathbb{D}_N \boldsymbol{\phi}, \mathbb{M}_{nn} \mathbf{w}\right)_{\partial \Omega} + \left(\mathbb{D}_N \boldsymbol{\phi}, \mathbb{M}_{nn} \mathbf{w}\right)_{\partial \Omega} = 0, \tag{95}$$

which is a symmetric bilinear form having the desired property. The relation (94) is equivalent to

$$SAT_{d2} = (JP)^{-1} \sum_{f \subset \partial \Omega} n_I \mathbb{D}_I e_f \hat{J} P_f e_f^T \left(\mathbb{M}_{nn} \mathbf{w} - \mathbf{g} \right).$$
 (96)

Next, we enforce (92) and (93) by writing $SAT_2 = SAT_{d3} + SAT_{cc}$. We require that SAT_{d3} satisfies

$$(\boldsymbol{\phi}, SAT_{d3})_{\Omega} = -(\boldsymbol{\phi}, \mathbb{V}_n \mathbf{w} - \mathbf{h})_{\partial\Omega},$$
 (97)

such that for h = 0, we obtain

$$B_{2}(\boldsymbol{\phi}, \mathbf{w}) = (\boldsymbol{\phi}, \mathbb{V}_{n} \mathbf{w})_{\partial \Omega} - (\boldsymbol{\phi}, \mathbb{V}_{n} \mathbf{w})_{\partial \Omega} - \sum_{\alpha} \boldsymbol{\phi}^{T} \left(\mathbb{M}_{\tau n} \mathbf{w} \Big|_{C_{0}^{\alpha}}^{C_{1}^{\alpha}} \right) + (\boldsymbol{\phi}, SAT_{cc})_{\partial \Omega}.$$
(98)

The relation (97) is equivalent to

$$SAT_{d3} = -(JP)^{-1} \sum_{f \subset \partial \Omega} e_f \hat{J} P_f e_f^T \left(\nabla_n \mathbf{w} - \mathbf{h} \right).$$
(99)

Finally, we require that SAT_{cc} satisfies

$$(\boldsymbol{\phi}, SAT_{cc})_{\Omega} = \sum_{\alpha} \boldsymbol{\phi}^{T} \left(\left(\mathbb{M}_{\tau n} \mathbf{w} - \mathbf{l}_{\mathbf{C}_{i}^{\alpha}} \right) \Big|_{C_{0}^{\alpha}}^{C_{1}^{\alpha}} \right),$$
 (100)

which is equivalent to the corner SAT terms, i.e.,

$$SAT_{cc} = (JP)^{-1} \sum_{\alpha} \left(\mathbb{M}_{\tau n} \mathbf{w} - \mathbf{l}_{\mathbf{C}_{\mathbf{i}}^{\alpha}} \right) \Big|_{C_0^{\alpha}}^{C_1^{\alpha}}.$$
 (101)

With these SAT terms, it follows that $B_2(\phi, \mathbf{w})$ vanishes for homogeneous boundary and corner conditions, as desired.

6.2. Clamped and free boundary conditions

Now consider clamped boundary conditions on $\partial \Omega_c$,

$$w = p,$$
 $\vec{X} \in \partial \Omega_c,$ $t \ge 0,$ (102)

$$n_I \partial_I w = q,$$
 $\vec{X} \in \partial \Omega_c$ $t \ge 0.$ (103)

and free boundary conditions (91), (92) on $\partial\Omega_f = \partial\Omega \setminus \partial\Omega_c$. Energy conservation can be obtained by imposing homogeneous conditions, e.g. g = h = l = p = q = 0. Recall that the discrete plate operator, without boundary SATs, is

$$\mathbb{D}_4 = -\mathbb{D}_2 \nu B \mathbb{D}_2 - \widetilde{\mathbb{D}}_J \widetilde{\mathbb{D}}_I (1 - \nu) B \mathbb{D}_I \mathbb{D}_J. \tag{104}$$

After imposing free boundary conditions on all free boundaries, the equation takes the form

$$m\ddot{\mathbf{w}} = \mathbb{D}_4 \mathbf{w} + \mathbb{S}_{d2} \left(\mathbb{M}_{nn} \mathbf{w} - \mathbf{g} \right) + \mathbb{S}_{d3} \left(\mathbb{V}_n \mathbf{w} - \mathbf{h} \right) + \mathbb{S}_{cc} \left(\mathbb{M}_{\tau n} \mathbf{w} - \mathbf{l} \right). \tag{105}$$

Gathering terms with \mathbf{w} and factorizing yields

$$m\ddot{\mathbf{w}} = \mathbb{D}_{4}^{f}\mathbf{w} - \mathbb{S}_{d2}\mathbf{g} - \mathbb{S}_{d3}\mathbf{h} - \mathbb{S}_{cc}\mathbf{l}, \tag{106}$$

where

$$\mathbb{D}_{4}^{f} = \mathbb{D}_{4} + \mathbb{S}_{d2}\mathbb{M}_{nn} + \mathbb{S}_{d3}\mathbb{V}_{n} + \mathbb{S}_{cc}\mathbb{M}_{\tau n}. \tag{107}$$

The SATs for free boundary conditions are such that \mathbb{D}_4^f satisfies

$$\mathbb{D}_{4}^{f} = -\mathbb{D}_{2}^{f} \nu B \mathbb{D}_{2} - \left(\widetilde{\mathbb{D}}_{J} \widetilde{\mathbb{D}}_{I}\right)^{f} (1 - \nu) B \mathbb{D}_{I} \mathbb{D}_{J}, \tag{108}$$

where \mathbb{D}_2^f and $\left(\widetilde{\mathbb{D}}_J\widetilde{\mathbb{D}}_I\right)^f$ satisfy the following formulas:

$$\left(\boldsymbol{\phi}, \mathbb{D}_{2}^{f} \mathbf{w}\right)_{\Omega} = \left(\boldsymbol{\phi}, \mathbb{D}_{N} \mathbf{w}\right)_{\partial \Omega_{c}} - \left(\mathbb{D}_{N} \boldsymbol{\phi}, \mathbf{w}\right)_{\partial \Omega_{c}} + \left(\mathbb{D}_{2} \boldsymbol{\phi}, \mathbf{w}\right)_{\Omega}, \tag{109}$$

and

$$\left(\boldsymbol{\phi}, \left(\widetilde{\mathbb{D}}_{J}\widetilde{\mathbb{D}}_{I}\right)^{f} \mathbf{w}\right)_{\Omega} = (\boldsymbol{\phi}, n_{J}\mathbb{D}_{I}\mathbf{w})_{\partial\Omega_{c}} - (\mathbb{D}_{J}\boldsymbol{\phi}, n_{I}\mathbf{w})_{\partial\Omega_{c}} + (\mathbb{D}_{I}\mathbb{D}_{J}\boldsymbol{\phi}, \mathbf{w})_{\Omega}.$$
(110)

We obtain the final operator after adding SATs for clamped boundary conditions:

$$\mathbb{D}_4^{fc} = \mathbb{D}_4^f + \mathbb{S}^c, \tag{111}$$

We seek a consistent \mathbb{S}^c such that \mathbb{D}_4^{fc} is symmetric negative semidefinite in the inner product, i.e.,

$$\left(\boldsymbol{\phi}, \mathbb{D}_{4}^{fc} \mathbf{w}\right)_{\Omega} = \left(\mathbb{D}_{4}^{fc} \boldsymbol{\phi}, \mathbf{w}\right)_{\Omega}, \quad \left(\mathbf{w}, \mathbb{D}_{4}^{fc} \mathbf{w}\right)_{\Omega} \leq 0,$$
 (112)

which ensures that the semi-discrete problem preserves a discrete energy (for p = q = 0), and hence is stable. Determining SAT^c may be arduous, and even for the significantly simpler beam operator, there is not a unique choice that leads to energy conservation. To identify a suitable SAT^c , we make the ansatz

$$\mathbb{D}_{4}^{fc} = -\mathbb{D}_{2}^{f} \nu B \mathbb{D}_{2}^{c} - \left(\widetilde{\mathbb{D}}_{J} \widetilde{\mathbb{D}}_{I}\right)^{f} (1 - \nu) B \left(\mathbb{D}_{I} \mathbb{D}_{J}\right)^{c}, \tag{113}$$

where

$$\mathbb{D}_{2}^{c} = \left(\mathbb{D}_{2}^{f}\right)^{\dagger}, \quad \left(\mathbb{D}_{I}\mathbb{D}_{J}\right)^{c} = \left(\left(\widetilde{\mathbb{D}}_{J}\widetilde{\mathbb{D}}_{I}\right)^{f}\right)^{\dagger}. \tag{114}$$

This ansatz guarantees that \mathbb{D}_4^{fc} is symmetric negative semidefinite, because

$$\left(\boldsymbol{\phi}, \mathbb{D}_{4}^{fc} \mathbf{w}\right)_{\Omega} = -\left(\boldsymbol{\phi}, \mathbb{D}_{2}^{f} \nu B \mathbb{D}_{2}^{c} \mathbf{w}\right)_{\Omega} - \left(\boldsymbol{\phi}, \left(\widetilde{\mathbb{D}}_{J} \widetilde{\mathbb{D}}_{I}\right)^{f} (1 - \nu) B \left(\mathbb{D}_{I} \mathbb{D}_{J}\right)^{c} \mathbf{w}\right)_{\Omega}
= -\left(\mathbb{D}_{2}^{c} \boldsymbol{\phi}, \nu B \mathbb{D}_{2}^{c} \mathbf{w}\right)_{\Omega} - \left(\left(\mathbb{D}_{I} \mathbb{D}_{J}\right)^{c} \boldsymbol{\phi}, (1 - \nu) B \left(\mathbb{D}_{I} \mathbb{D}_{J}\right)^{c} \mathbf{w}\right)_{\Omega},$$
(115)

and hence the operator \mathbb{D}_4^{fc} is stable. It remains to show that the corresponding SAT^c is consistent with clamped boundary conditions. We have

$$(\boldsymbol{\phi}, SAT^{c}\mathbf{w})_{\Omega} = \left(\boldsymbol{\phi}, \left(\mathbb{D}_{4}^{f} - \mathbb{D}_{4}^{fc}\right)\mathbf{w}\right)_{\Omega}$$

$$= -\left(\boldsymbol{\phi}, \mathbb{D}_{2}^{f}\nu B\left(\mathbb{D}_{2} - \mathbb{D}_{2}^{c}\right)\mathbf{w}\right)_{\Omega}$$

$$-\left(\boldsymbol{\phi}, \left(\widetilde{\mathbb{D}}_{J}\widetilde{\mathbb{D}}_{I}\right)^{f} (1 - \nu)B\left(\mathbb{D}_{I}\mathbb{D}_{J} - (\mathbb{D}_{I}\mathbb{D}_{J})^{c}\right)\mathbf{w}\right)_{\Omega}$$

$$= -\left(\nu B\mathbb{D}_{2}^{c}\boldsymbol{\phi}, (\mathbb{D}_{2} - \mathbb{D}_{2}^{c})\mathbf{w}\right)_{\Omega} - \left((1 - \nu)B\left(\mathbb{D}_{I}\mathbb{D}_{J}\right)^{c}\boldsymbol{\phi}, (\mathbb{D}_{I}\mathbb{D}_{J} - (\mathbb{D}_{I}\mathbb{D}_{J})^{c}\right)\mathbf{w}\right)_{\Omega}.$$
(116)

To proceed, note that

$$\left(\boldsymbol{\phi}, \mathbb{D}_{2}^{c} \mathbf{w}\right)_{\Omega} = \left(\boldsymbol{\phi}, \left(\mathbb{D}_{2}^{f}\right)^{\dagger} \mathbf{w}\right)_{\Omega} = -(\boldsymbol{\phi}, \mathbb{D}_{N} \mathbf{w})_{\partial \Omega_{c}} + (\mathbb{D}_{N} \boldsymbol{\phi}, \mathbf{w})_{\partial \Omega_{c}} + (\boldsymbol{\phi}, \mathbb{D}_{2} \mathbf{w})_{\Omega}, \qquad (117)$$

and

$$(\boldsymbol{\phi}, (\mathbb{D}_J \mathbb{D}_I)^c \mathbf{w})_{\Omega} = \left(\boldsymbol{\phi}, \left(\left(\widetilde{\mathbb{D}}_J \widetilde{\mathbb{D}}_I \right)^f \right)^\dagger \mathbf{w} \right)_{\Omega} = (n_J \mathbb{D}_I \boldsymbol{\phi}, \mathbf{w})_{\partial \Omega_c} - (n_I \boldsymbol{\phi}, \mathbb{D}_J \mathbf{w})_{\partial \Omega_c} + (\boldsymbol{\phi}, \mathbb{D}_I \mathbb{D}_J \mathbf{w})_{\Omega}.$$

$$(118)$$

Using (117) and (118) in (116) yields

$$(\boldsymbol{\phi}, SAT^{c}\mathbf{w})_{\Omega} = -(\nu B \mathbb{D}_{2}^{c} \boldsymbol{\phi}, \mathbb{D}_{N}\mathbf{w})_{\partial\Omega_{c}} + (\mathbb{D}_{N}\nu B \mathbb{D}_{2}^{c} \boldsymbol{\phi}, \mathbf{w})_{\partial\Omega_{c}} + (n_{J}\mathbb{D}_{I}(1-\nu)B(\mathbb{D}_{I}\mathbb{D}_{J})^{c} \boldsymbol{\phi}, \mathbf{w})_{\partial\Omega_{c}} - (n_{I}(1-\nu)B(\mathbb{D}_{I}\mathbb{D}_{J})^{c} \boldsymbol{\phi}, \mathbb{D}_{J}\mathbf{w})_{\partial\Omega_{c}}.$$
(119)

Recall the formula

$$(\boldsymbol{\phi}, \mathbb{D}_{I}\mathbf{w})_{\Gamma} = (\boldsymbol{\phi}, n_{I}\mathbb{D}_{N} + \tau_{I}\mathbb{D}_{T}\mathbf{w})_{\Gamma} = (\boldsymbol{\phi}, n_{I}\mathbb{D}_{N}\mathbf{w})_{\Gamma} + \sum_{\alpha} \boldsymbol{\phi}^{T}\tau_{I}\left(\mathbf{w}\Big|_{C_{0}^{\alpha}}^{C_{1}^{\alpha}}\right) - (\mathbb{D}_{T}\tau_{I}\boldsymbol{\phi}, \mathbf{w})_{\Gamma}.$$
(120)

The last term on the right-hand side of (119) can be re-written as

$$-\left(n_{I}(1-\nu)B\left(\mathbb{D}_{I}\mathbb{D}_{J}\right)^{c}\boldsymbol{\phi},\mathbb{D}_{J}\mathbf{w}\right)_{\partial\Omega_{c}} = -\sum_{\alpha}\left(n_{I}(1-\nu)B\left(\mathbb{D}_{I}\mathbb{D}_{J}\right)^{c}\boldsymbol{\phi}\right)^{T}\tau_{J}\left(\mathbf{w}\Big|_{C_{0}^{\alpha}}^{C_{1}^{\alpha}}\right) + \left(\mathbb{D}_{T}\tau_{J}n_{I}(1-\nu)B\left(\mathbb{D}_{I}\mathbb{D}_{J}\right)^{c}\boldsymbol{\phi},\mathbf{w}\right)_{\partial\Omega_{c}} - \left(n_{J}n_{I}(1-\nu)B\left(\mathbb{D}_{I}\mathbb{D}_{J}\right)^{c}\boldsymbol{\phi},\mathbb{D}_{N}\mathbf{w}\right)_{\partial\Omega_{c}}.$$

$$(121)$$

We obtain

$$(\boldsymbol{\phi}, SAT^{c}\mathbf{w})_{\Omega} = -(\nu B \mathbb{D}_{2}^{c} \boldsymbol{\phi}, \mathbb{D}_{N}\mathbf{w})_{\partial\Omega_{c}} + (\mathbb{D}_{N}\nu B \mathbb{D}_{2}^{c} \boldsymbol{\phi}, \mathbf{w})_{\partial\Omega_{c}} + (n_{J}\mathbb{D}_{I}(1-\nu)B(\mathbb{D}_{I}\mathbb{D}_{J})^{c} \boldsymbol{\phi}, \mathbf{w})_{\partial\Omega_{c}} - \sum_{\alpha} (n_{I}(1-\nu)B(\mathbb{D}_{I}\mathbb{D}_{J})^{c} \boldsymbol{\phi})^{T} \tau_{J} \left(\mathbf{w} \Big|_{C_{0}^{\alpha}}^{C_{1}^{\alpha}}\right) + (\mathbb{D}_{T}\tau_{J}n_{I}(1-\nu)B(\mathbb{D}_{I}\mathbb{D}_{J})^{c} \boldsymbol{\phi}, \mathbf{w})_{\partial\Omega_{c}} - (n_{J}n_{I}(1-\nu)B(\mathbb{D}_{I}\mathbb{D}_{J})^{c} \boldsymbol{\phi}, \mathbb{D}_{N}\mathbf{w})_{\partial\Omega_{c}}.$$
(122)

Gathering terms leads to

$$(\boldsymbol{\phi}, SAT^{c}\mathbf{w})_{\Omega} = -\left((\nu B \mathbb{D}_{2}^{c} + n_{J} n_{I} (1 - \nu) B \left(\mathbb{D}_{I} \mathbb{D}_{J}\right)^{c}\right) \boldsymbol{\phi}, \mathbb{D}_{N} \mathbf{w})_{\partial \Omega_{c}} + \left((\mathbb{D}_{N} \nu B \mathbb{D}_{2}^{c} + (n_{J} \mathbb{D}_{I} + \mathbb{D}_{T} \tau_{J} n_{I}) (1 - \nu) B \left(\mathbb{D}_{I} \mathbb{D}_{J}\right)^{c}\right) \boldsymbol{\phi}, \mathbf{w})_{\partial \Omega_{c}} - \sum_{\alpha} \left(n_{I} (1 - \nu) B \left(\mathbb{D}_{I} \mathbb{D}_{J}\right)^{c} \boldsymbol{\phi}\right)^{T} \tau_{J} \left(\mathbf{w} \Big|_{C_{0}^{\alpha}}^{C_{1}^{\alpha}}\right).$$

$$(123)$$

This shows that SAT^c is consistent with clamped boundary conditions and $SAT^c = SAT_{d1} + SAT_c$, where, for inhomogeneous conditions,

$$SAT_{d1} = -\sum_{f \subset \partial \Omega_c} \left[(\mathbb{D}_2^c)^T \nu B P^{-1} e_f \hat{J} P_f e_f^T \right] (\mathbb{D}_N \mathbf{w} - \mathbf{h})$$

$$+ \sum_{f \subset \partial \Omega_c} \left[((\mathbb{D}_I \mathbb{D}_J)^c)^T P^{-1} (1 - \nu) B e_f \hat{J} P_f e_f^T n_I n_J \right] (\mathbb{D}_N \mathbf{w} - \mathbf{h})$$
(124)

and

$$SAT_{e} = \sum_{f \subset \partial \Omega} \left[(\mathbb{D}_{2}^{c})^{T} \nu B P^{-1} \mathbb{D}_{N} e_{f} \hat{J} P_{f} e_{f}^{T} \right] (\mathbf{w} - \mathbf{g})$$

$$+ \sum_{f \subset \partial \Omega} ((\mathbb{D}_{I} \mathbb{D}_{J})^{c})^{T} P^{-1} (1 - \nu) B \left(\mathbb{D}_{I} e_{f} \hat{J} P_{f} e_{f}^{T} n_{J} + n_{I} \tau_{J} \mathbb{D}_{T}^{T} e_{f} \hat{J} P_{f} e_{f}^{T} \right) (\mathbf{w} - \mathbf{g})$$

$$- \sum_{\alpha} ((\mathbb{D}_{I} \mathbb{D}_{J})^{c})^{T} P^{-1} (1 - \nu) B n_{T} \tau_{J} \left((\mathbf{w} - \mathbf{g}) \Big|_{C_{0}^{\alpha}}^{C_{1}^{\alpha}} \right).$$

$$(125)$$

Note that the summation over α here is performed on clamped boundary segments only.

6.3. Self-adjointness

In PDE-constrained optimization problems the adjoint of the discrete operator plays an important role. Computing the gradient of the objective functional usually requires the adjoint state method. Our objective in this subsection is to prove that the discrete plate operator is self-adjoint, just like its corresponding continuous operator. As a consequence of this property, one can use the same solver for both the forward and adjoint problems and obtain the exact gradient of a discrete objective functional up to roundoff error (given that the time-discretization is also self-adjoint).

Here we consider the plate operator $\mathcal{D}_4 = \partial_J \partial_I M_{IJ}$. The domain of \mathcal{D}_4 is unspecified for now. We define the space of admissible functions

$$W = \left\{ w \in L^2(\Omega) \middle| \mathcal{D}_4 w \in L^2(\Omega) \right\}. \tag{126}$$

Furthermore, we assume that w satisfies either free boundary and corner conditions ((91), (92), (93)) or clamped boundary conditions ((102), (103)). Let W_F and W_C denote the corresponding spaces:

$$\mathcal{W}_{F} = \left\{ w \in \mathcal{W} \middle| M_{nn} w = 0, V_{n} w = 0 \text{ on } \partial \Omega, M_{\tau n} w \middle|_{\vec{X} = C_{i}^{\alpha}} = 0, \forall \alpha \text{ and } i \in \{0, 1\} \right\}, \\
\mathcal{W}_{C} = \left\{ w \in \mathcal{W} \middle| w = 0, n_{I} \partial_{I} w = 0 \text{ on } \partial \Omega \right\}.$$
(127)

Integration by parts (73) yields

$$(\phi, \mathcal{D}_{4}w)_{\Omega} = (\phi, V_{n}w)_{\partial\Omega} - (\mathcal{D}_{n}\phi, M_{nn}w)_{\partial\Omega} - \sum_{\alpha} \phi M_{\tau n}w \Big|_{C_{0}^{\alpha}}^{C_{1}^{\alpha}}$$

$$- (\mathcal{D}_{2}\phi, \nu B\mathcal{D}_{2}w)_{\Omega} - (\mathcal{D}_{I}\mathcal{D}_{J}\phi, (1-\nu)B\mathcal{D}_{I}\mathcal{D}_{J}w)_{\Omega}$$

$$= - (\mathcal{D}_{2}\phi, \nu B\mathcal{D}_{2}w)_{\Omega} - (\mathcal{D}_{I}\mathcal{D}_{J}\phi, (1-\nu)B\mathcal{D}_{I}\mathcal{D}_{J}w)_{\Omega}$$

$$= - (\nu B\mathcal{D}_{2}\phi, \mathcal{D}_{2}w)_{\Omega} - ((1-\nu)B\mathcal{D}_{I}\mathcal{D}_{J}\phi, \mathcal{D}_{I}\mathcal{D}_{J}w)_{\Omega}$$

$$= (\mathcal{D}_{4}\phi, w)_{\Omega} \qquad \forall w, \phi \in \mathcal{W}_{F} \text{ or } \forall w, \phi \in \mathcal{W}_{C},$$

$$(128)$$

which shows that \mathcal{D}_4 is self-adjoint both with domain \mathcal{W}_F (free with corner conditions) and with domain \mathcal{W}_C (clamped conditions).

We now consider the total discrete elastic operator, including SATs. Assuming homogeneous boundary and corner conditions, we can define S such that

$$SAT = \mathbb{S}\mathbf{w},\tag{129}$$

and the total discrete operator is

$$\mathbb{D}_4^{tot} = \mathbb{D}_4 + \mathbb{S}. \tag{130}$$

Theorem 4. The total discrete elastic operator, including SATs for free with corner or clamped boundary conditions, is self-adjoint, i.e.,

$$(\boldsymbol{\phi}, \mathbb{D}_4^{tot} \mathbf{w})_{\Omega} = (\mathbb{D}_4^{tot} \boldsymbol{\phi}, \mathbf{w})_{\Omega} \quad \forall \boldsymbol{\phi}, \mathbf{w}. \tag{131}$$

Proof. First, consider the case with free boundary conditions. In deriving the weak form (88), we showed that

$$\left(\boldsymbol{\phi}, \mathbb{D}_{4}^{tot}\mathbf{w}\right)_{\Omega} = -K\left(\boldsymbol{\phi}, \mathbf{w}\right) + B\left(\boldsymbol{\phi}, \mathbf{w}\right),$$
 (132)

where K is symmetric and B is symmetric both in the case of free boundary and corner conditions (cf. (95), (98)) Hence, we have

$$\left(\boldsymbol{\phi}, \mathbb{D}_{4}^{tot}\mathbf{w}\right)_{\Omega} = -K\left(\boldsymbol{\phi}, \mathbf{w}\right) + B\left(\boldsymbol{\phi}, \mathbf{w}\right) = -K\left(\mathbf{w}, \boldsymbol{\phi}\right) + B\left(\mathbf{w}, \boldsymbol{\phi}\right) = \left(\mathbf{w}, \mathbb{D}_{4}^{tot}\boldsymbol{\phi}\right)_{\Omega}. \tag{133}$$

The result follows after using the symmetry of $(\cdot, \cdot)_{\Omega}$.

As for mixed clamped and free boundary conditions, the operator is self-adjoint by construction (cf. (112)).

7. Ice shelf covered ocean model

In this section, we couple the plate equation with the shallow water equation. In this study, we consider a 2D domain Ω as in Fig. 3. The governing equations are

$$\dot{w} + \partial_I H \partial_I \phi = 0, \qquad \qquad \vec{X} \in \Omega, \qquad \qquad t \ge 0, \qquad (134a)$$

$$m\ddot{w} - \partial_J \partial_I M_{IJ} w = -\rho_w (\dot{\phi} + gw), \qquad \vec{X} \in \Omega, \qquad \qquad t \ge 0, \qquad (134b)$$

$$n_I \partial_I \phi = 0, \qquad \qquad \vec{X} \in \partial \Omega, \qquad \qquad t \ge 0, \qquad (134c)$$

$$w = 0, \qquad \qquad \vec{X} \in \partial \Omega_E \cup \partial \Omega_N, \qquad t \ge 0, \qquad (134d)$$

$$n_I \partial_I w = 0, \qquad \qquad \vec{X} \in \partial \Omega_E \cup \partial \Omega_N, \qquad t \ge 0, \qquad (134e)$$

$$M_{nn} w = 0, \qquad \qquad \vec{X} \in \partial \Omega_W \cup \partial \Omega_S, \qquad t \ge 0, \qquad (134f)$$

$$V_n w = 0, \qquad \qquad \vec{X} \in \partial \Omega_W \cup \partial \Omega_S, \qquad t \ge 0, \qquad (134g)$$

$$M_{\tau n} w = 0, \qquad \qquad \vec{X} \in \{SE, NW\} \qquad t \ge 0, \qquad (134h)$$

in which $\phi(\vec{X},t)$ is the velocity potential, $H(\vec{X})$ is the water depth, ρ_w is the water density, and g is the gravitational acceleration. From the velocity potential, we can calculate horizontal particle velocities as $\partial_I \phi$ and pressure perturbation as $-\rho_w \dot{\phi}$. Thus (134a) expresses depth-integrated conservation of mass for the incompressible water and the right side of (134b) sets the vertical load applied to the plate equal to the wave-induced pressure perturbation, including a term $(\rho_w gw)$ corresponding to hydrostatic pressure change induced by vertical displacement of the water surface.

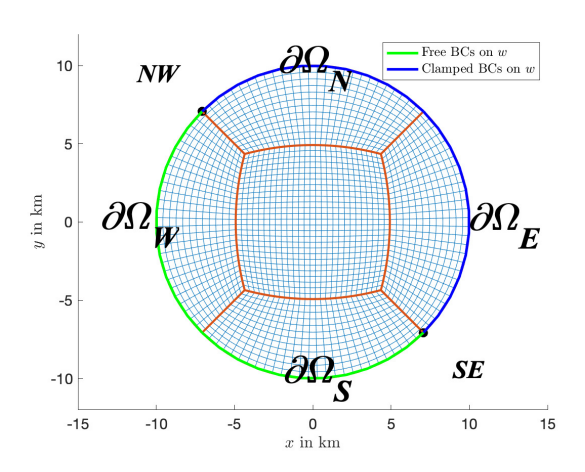


Figure 3: Domain and grid configuration

7.1. Continuous problem weak form and energy balance

The weak formulation for the shallow water equation is obtained by multiplying (134a) by $\rho_w \chi$, integrating over Ω , and integrating by parts:

$$(\rho_w \chi, \dot{w})_{\Omega} = -(\rho_w \chi, \partial_I H \partial_I \phi)_{\Omega} = (\rho_w \partial_I \chi, H \partial_I \phi)_{\Omega} - (\rho_w \chi, H n_I \partial_I \phi)_{\partial\Omega}.$$
(135)

We define the kinetic energy of the water as

$$\mathcal{E}_W = \frac{1}{2} \left(\partial_I \phi, \rho_w H \partial_I \phi \right)_{\Omega}, \tag{136}$$

which allows us to set $\chi = \dot{\phi}$ in (135) to obtain the energy balance of the water:

$$\frac{\mathrm{d}\mathcal{E}_W}{\mathrm{d}t} = \left(\rho_w \dot{\phi}, \dot{w}\right)_{\Omega} + \left(n_I \partial_I \phi, \rho_w H \dot{\phi}\right)_{\partial\Omega}.$$
 (137)

Next, taking the inner product of (134b) with ψ and using integration-by-parts as in (19), we obtain the weak form:

$$(m\psi, \ddot{w})_{\Omega} + (\partial_{I}\partial_{J}\psi, -M_{IJ}w)_{\Omega} + (\psi, \rho_{w}gw)_{\Omega} = (\psi, V_{n}w)_{\partial\Omega} - (n_{I}\partial_{I}\psi, M_{nn}w)_{\partial\Omega} - \sum_{\alpha} [\psi M_{\tau n}w]_{C_{0}^{\alpha}}^{C_{1}^{\alpha}} - (\psi, \rho_{w}\dot{\phi})_{\Omega}.$$

$$(138)$$

Then we set $\psi = \dot{w}$ and using (21), we obtain the plate energy balance

$$\frac{\mathrm{d}\mathcal{E}}{\mathrm{d}t} + (\dot{w}, \rho_w g w)_{\Omega} = -\left(\dot{w}, \rho_w \dot{\phi}\right)_{\Omega}.$$
(139)

We then define the total energy of the system as the sum of \mathcal{E} (the kinetic and strain energy of the plate), the kinetic energy of the water \mathcal{E}_W , and the gravitational potential energy:

$$\mathcal{E}_{tot} = \mathcal{E} + \mathcal{E}_W + \frac{1}{2} (w, \rho_w g w)_{\Omega}. \tag{140}$$

and combining the previous equations shows that total energy is conserved:

$$\frac{\mathrm{d}\mathcal{E}_{tot}}{\mathrm{d}t} = 0. \tag{141}$$

7.2. Discretization

We discretize (134a) and (134b) as

$$\dot{\mathbf{w}} = -\mathbb{D}_2(H)\boldsymbol{\phi} + SAT_{\boldsymbol{\phi}},\tag{142a}$$

$$m\ddot{\mathbf{w}} + \rho_w \dot{\boldsymbol{\phi}} = \mathbb{D}_4 \mathbf{w} - \rho_w q \mathbf{w} + SAT_{\mathbf{w}}. \tag{142b}$$

As in section 6, the weak form is obtained by multiplying (142a) by $\rho_w \chi^T JP$:

$$(\rho_{w}\dot{\boldsymbol{\chi}}, \dot{\mathbf{w}})_{\Omega} = -(\rho_{w}\dot{\boldsymbol{\chi}}, \mathbb{D}_{2}(H)\boldsymbol{\phi})_{\Omega} + (\rho_{w}\boldsymbol{\chi}, SAT_{\boldsymbol{\phi}})_{\Omega}$$

$$= (\mathbb{D}_{I}\dot{\boldsymbol{\chi}}, \rho_{w}H\mathbb{D}_{I}\boldsymbol{\phi})_{\Omega} - \left(n_{I}\mathbb{D}_{I}\boldsymbol{\chi}, \rho_{w}H\dot{\boldsymbol{\phi}}\right)_{\partial\Omega} + (\rho_{w}\boldsymbol{\chi}, SAT_{\boldsymbol{\phi}})_{\Omega}$$

$$= 23$$
(143)

and by multiplying (142b) by $\psi^T JP$:

$$(m\boldsymbol{\psi}, \ddot{\mathbf{w}})_{\Omega} + (\boldsymbol{\psi}, \rho_{w}\dot{\boldsymbol{\phi}})_{\Omega} = (\boldsymbol{\psi}, \mathbb{D}_{4}\mathbf{w})_{\Omega} - (\boldsymbol{\psi}, \rho_{w}g\mathbf{w})_{\Omega} + (\boldsymbol{\psi}, SAT_{w})_{\Omega}$$

$$= -(\mathbb{D}_{2}\boldsymbol{\psi}, \nu B\mathbb{D}_{2}\mathbf{w})_{\Omega} - (\mathbb{D}_{I}\mathbb{D}_{J}\boldsymbol{\psi}, (1-\nu)B\mathbb{D}_{I}\mathbb{D}_{J}\mathbf{w})_{\Omega} - (\boldsymbol{\psi}, \rho_{w}g\mathbf{w})_{\Omega}$$

$$+ (\boldsymbol{\psi}, \mathbb{V}_{n}\mathbf{w})_{\partial\Omega} - (\mathbb{D}_{N}\boldsymbol{\psi}, \mathbb{M}_{nn}\mathbf{w})_{\partial\Omega} - \sum_{\alpha} \boldsymbol{\psi}^{T} \left(\mathbb{M}_{\tau n}\mathbf{w} \Big|_{C_{0}^{\alpha}}^{C_{1}^{\alpha}}\right)$$

$$+ (\boldsymbol{\psi}, SAT_{w})_{\Omega}.$$

$$(144)$$

To obtain the energy balance for the semi-discrete problem, set $\chi = \phi$ in (143):

$$\frac{1}{2}\frac{\mathrm{d}}{\mathrm{d}t}\left(\mathbb{D}_{I}\boldsymbol{\phi},\rho_{w}H\mathbb{D}_{I}\boldsymbol{\phi}\right)_{\Omega} = \left(\rho_{w}\dot{\boldsymbol{\phi}},\dot{\mathbf{w}}\right)_{\Omega} + BT_{1}$$
(145)

and $\psi = \dot{\mathbf{w}}$ in (144):

$$\frac{1}{2} \frac{\mathrm{d}}{\mathrm{d}t} \left[(\mathbb{D}_{2} \mathbf{w}, \nu B \mathbb{D}_{2} \mathbf{w})_{\Omega} + (\mathbb{D}_{I} \mathbb{D}_{J} \mathbf{w}, (1 - \nu) B \mathbb{D}_{I} \mathbb{D}_{J} \mathbf{w})_{\Omega} + (\mathbf{w}, \rho_{w} g \mathbf{w})_{\Omega} + (m \dot{\mathbf{w}}, \dot{\mathbf{w}})_{\Omega} \right] \\
= - \left(\dot{\mathbf{w}}, \rho_{w} \dot{\boldsymbol{\phi}} \right)_{\Omega} + B T_{2}, \tag{146}$$

and add:

$$\frac{1}{2}\frac{d}{dt}E = BT_1 + BT_2 = BT, (147)$$

where the discrete total energy is

$$E = \frac{1}{2} [(\mathbb{D}_{I} \boldsymbol{\phi}, \rho_{w} H \mathbb{D}_{I} \boldsymbol{\phi})_{\Omega} + (\mathbf{w}, \rho_{w} g \mathbf{w})_{\Omega} + (m \dot{\mathbf{w}}, \dot{\mathbf{w}})_{\Omega}]$$

$$+ \frac{1}{2} [(\mathbb{D}_{2} \mathbf{w}, \nu B \mathbb{D}_{2} \mathbf{w})_{\Omega} + (\mathbb{D}_{I} \mathbb{D}_{J} \mathbf{w}, (1 - \nu) B \mathbb{D}_{I} \mathbb{D}_{J} \mathbf{w})_{\Omega}]$$

$$(148)$$

and boundary terms

$$BT = -\left(n_{I}\mathbb{D}_{I}\boldsymbol{\phi}, \rho_{w}H\dot{\boldsymbol{\phi}}\right)_{\partial\Omega} + \left(\rho_{w}\boldsymbol{\phi}, SAT_{\boldsymbol{\phi}}\right)_{\Omega} + \left(\dot{\mathbf{w}}, \mathbb{V}_{n}\mathbf{w}\right)_{\partial\Omega} - \left(\mathbb{D}_{N}\dot{\mathbf{w}}, \mathbb{M}_{nn}\mathbf{w}\right)_{\partial\Omega} - \sum_{\alpha} \dot{\mathbf{w}}^{T} \left(\mathbb{M}_{\tau n}\mathbf{w}\Big|_{C_{0}^{\alpha}}^{C_{1}^{\alpha}}\right) + \left(\dot{\mathbf{w}}, SAT_{w}\right)_{\Omega}.$$

$$(149)$$

Now, let us reinstate the total operators that incorporate SBP-SAT boundary terms

$$\mathbb{D}_4^{tot}\mathbf{w} = \mathbb{D}_4\mathbf{w} + \mathbb{S}_\mathbf{w}\mathbf{w} = \mathbb{D}_4\mathbf{w} + SAT_\mathbf{w}$$
 (150)

and

$$\mathbb{D}_{2}^{tot} \boldsymbol{\phi} = \mathbb{D}_{2} \boldsymbol{\phi} + \mathbb{S}_{\boldsymbol{\phi}} = \mathbb{D}_{2} \boldsymbol{\phi} + SAT_{\boldsymbol{\phi}}. \tag{151}$$

Using the total operators, insert (142a) into (142b)

$$\dot{\mathbf{w}} = -\mathbb{D}_2^{tot}(H)\boldsymbol{\phi}, -m\mathbb{D}_2^{tot}(H)\dot{\boldsymbol{\phi}} + \rho_w \dot{\boldsymbol{\phi}} = \mathbb{D}_4^{tot} \mathbf{w} - \rho_w g \mathbf{w}.$$
 (152)

The semi-discrete system can be written as

$$\begin{bmatrix} \mathbb{I} & & & \\ & (-m\mathbb{D}_2^{tot}(H) + \rho_w \mathbb{I}) \end{bmatrix} \begin{bmatrix} \mathbf{w} \\ \boldsymbol{\phi} \end{bmatrix}_t = \begin{bmatrix} & & -\mathbb{D}_2^{tot}(H) \\ \mathbb{D}_4^{tot} - \rho_w g \mathbb{I} \end{bmatrix} \begin{bmatrix} \mathbf{w} \\ \boldsymbol{\phi} \end{bmatrix}. \tag{153}$$

We will be solving (153).

8. Numerical experiments

This section consists of two numerical experiments. First, the method of manufactured solutions is used to assess the global convergence rates of the new SBP-SAT schemes, implemented using Mattson's variable coefficient SBP operators [21]. Second, we solve an application problem inspired by ocean wave interaction with ice shelves off the coast of West Antarctica. For both experiments we use a system of self-consistent units (Table 1) such that the discretization matrices are not ill-conditioned.

Field	Units				
x, y	$10^3 \mathrm{m}$				
w	\mathbf{m}				
t	\mathbf{s}				
ϕ	$10^3 \ {\rm m^2/s}$				
H, h	$10^3 \mathrm{m}$				
ρ_i, ρ_w	$10^3 \mathrm{\ kg/m^3}$				
m	$10^6 \mathrm{\ kg/m^2}$				
g	$10^3 \mathrm{\ m/s^2}$				
B	10^{18} Pa m^3				
p	MPa				

Since the system of equations (153) is very stiff, it is beneficial to use an implicit timeintegration method. We here opt for the second-order Crank-Nicolson method. Even though the method is unconditionally stable, we should pick the time step Δt to keep accuracy. Therefore, we pick the time step according to

$$\Delta t = \text{const.} \times \sqrt{\frac{m_0}{B_0}} (\Delta x)^2,$$
 (154)

where m_0 and B_0 are nominal values of m and B, respectively, and Δx is the grid spacing. This choice is inspired by the dispersion relation for flexural waves in a plate.

8.1. Convergence studies

We use the method of manufactured solutions on the domain depicted in Fig. 3 and choose the exact solution

$$w(x, y, t) = W_0 \cos(k_1 x + k_2 y + \omega t), \quad \phi(x, y, t) = \Phi_0 \sin(k_1 x + k_2 y + \omega t), \quad (155)$$

where

$$W_0 = 0.01, \quad \Phi_0 = -W_0 \frac{\omega}{H_0 k^2}, \quad k = \frac{2\pi}{\lambda} = \sqrt{k_1^2 + k_2^2}$$
 (156)

and

$$\omega = k\sqrt{H_0 \frac{B_0 k^4 + \rho_w g}{\rho_w + H_0 k^2 m_0}} \tag{157}$$

with

$$(k_1, k_2) = (k \cos \alpha, k \sin \alpha) \tag{158}$$

and

$$\lambda = \frac{8 \times 2 \times 0.435 \times R}{18} \approx 3.867 \text{km}.$$
 (159)

The choice of λ is such that the number of points per wavelength (PPWL) is above 8. The angular velocity ω and the amplitudes W_0 and Φ_0 are chosen by solving the dispersion relation with the following constant material parameters: $\nu = 0.3$, $m_0 = (0.3\rho_i) \times 10^6 \text{kg/m}^2$, $H_0 = 0.6 \text{km}$ and $B_0 = (0.3)^3 \times 10^{18} \text{Pa m}^3$. We choose the propagation angle $\alpha = \frac{\pi}{4}$. The material parameters are

$$\nu(x,y) = \nu_0 \left(1 - \frac{1}{3} \sin \left(\frac{x+3y}{R} \right) \right), \tag{160}$$

$$m(x,y) = m_0 \left(1 + \frac{1}{3} \sin \left(\frac{x+3y}{R} \right) \right), \tag{161}$$

$$H(x,y) = H_0 \left(1 - \frac{1}{3} \sin \left(\frac{x+3y}{R} \right) \right) \tag{162}$$

and

$$B(x,y) = \left(\frac{m(x,y)}{\rho_i}\right)^3 \tag{163}$$

with R = 10 km.

We impose free boundary conditions on the East and North boundaries and clamped boundaries on the West and South boundaries, and use the exact solution as boundary and initial data. We use the Crank-Nicolson method for time-integration. We set $T = 2\pi/\omega \approx 13.45$ s as the final time. The Crank-Nicolson method requires solving a linear system at each time step. For that, we use MATLAB's GMRES iterative solver with a tolerance of 10^{-9} , maximum iteration of 300, and incomplete LU-decomposition ilu() as preconditioners. For Ilu() we select: type is 'crout', droptol is 10^{-5} , milu is 'row'. Table 1 and Fig. 4 show the relative l^2 errors as functions of Δx , where Δx denotes the average grid spacing in the physical domain. Table 1 also shows the number of grid points per wavelength (PPWL) used in the inner domain. The convergence rates appear to be approaching rates of 2, 3.5 and 4.5 for interior orders of 2q = 2, 4, 6, respectively, which are the rates that have been observed for anisotropic problems [2].

Table 1: l^2 errors and convergence rates r

Δx	PPWL	Second order		Fourth order		Sixth order	
		$\log_{10}(\text{error})$	r	$\log_{10}(\text{error})$	r	$\log_{10}(\text{error})$	r
0.2122	18	-0.81		-2.16		-2.49	
0.1706	23	-1.01	2.11	-2.53	3.91	-2.99	5.27
0.1426	27	-1.16	1.94	-2.80	3.54	-3.37	4.87
0.1225	32	-1.30	2.11	-3.04	3.63	-3.67	4.64
0.1074	36	-1.41	1.94	-3.24	3.46	-3.96	4.96
0.0956	40	-1.51	1.94	-3.41	3.29	-4.17	4.17
Avg. rate			2.01		3.56		4.78

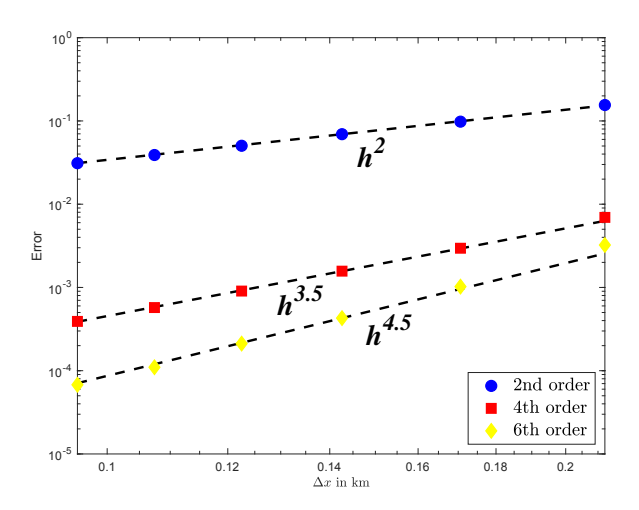


Figure 4: Convergence plot

8.2. Stability and self-adjointness

We use the domain in Fig. 3 again to verify that the scheme for the plate equation is energy conserving and self-adjoint. The total discrete plate operator \mathbb{D}_4^{tot} is self-adjoint in the inner product defined by the physical quadrature JP (131). In our case, this is equivalent to the matrix A being symmetric, where

$$A = JP \mathbb{D}_{4}^{tot} \tag{164}$$

By setting the smallest grid spacing in the physical domain to $\Delta x = 0.0956$, we obtain a total of 23,552 grid points. The relative deviations from symmetry $||A - A^T||_{\text{max}}/||A||_{\text{max}}$ for this problem (using double precision floating point operations) are:

2nd order:
$$7.76 \times 10^{-15}$$
, 4th order: 9.93×10^{-15} , 6th order: 3.32×10^{-15} ,

which verifies that the schemes are self-adjoint to machine precision.

Without external forces and boundary data, the semi-discrete equations become

$$\rho_w J P \dot{\mathbf{w}} + \rho_w J P \mathbb{D}_2^{tot}(H) \boldsymbol{\phi} = 0$$

$$m J P \dot{\mathbf{w}} = A \mathbf{w} - \rho_w q J P \mathbf{w} - \rho_w J P \boldsymbol{\phi}.$$
(165)

Since A is symmetric, the semidiscrete problem preserves the quantity

$$\varepsilon_{tot} = \frac{1}{2} \left((\dot{\mathbf{w}})^T m J P \dot{\mathbf{w}} - \mathbf{w}^T A \mathbf{w} + \mathbf{w}^T \rho_w g J P \mathbf{w} + \rho_w \boldsymbol{\phi}^T J P \mathbb{D}_2^{tot}(H) \boldsymbol{\phi} \right),$$

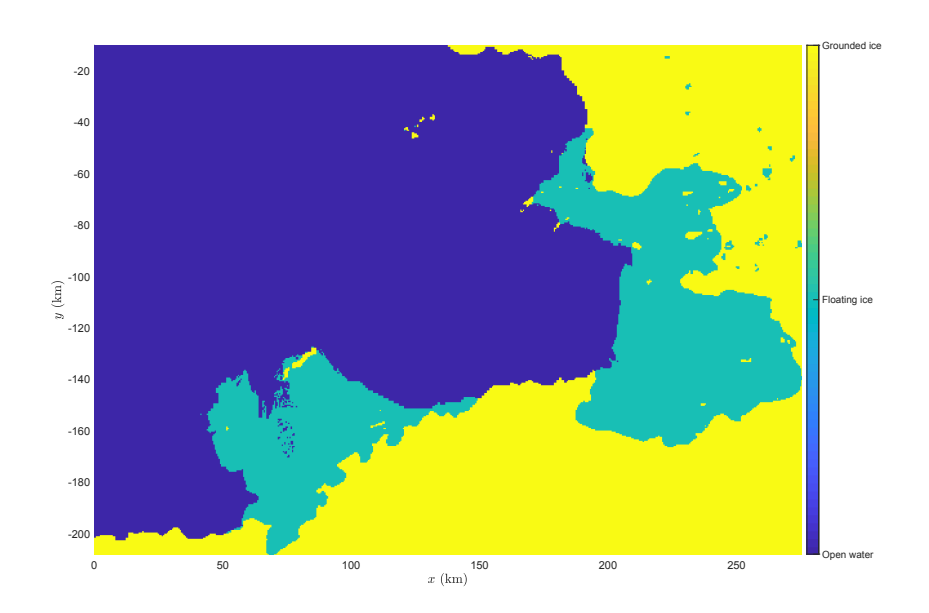


Figure 5: BedMachine Version 2 mask of Amundsen Sea Region

which is the same semidiscrete energy given by (140). Furthermore, our stability analysis guarantees that the semidiscrete energy is non-negative, and hence a seminorm of \mathbf{w} , which means that with proper SATs, A is negative semidefinite. For the current problem, the largest eigenvalues of A are:

2nd order: -2.0933×10^{-7} , 4th order: -2.0927×10^{-7} , 6th order: -2.0934×10^{-7} , which verifies that A is negative semidefinite.

8.3. Ocean wave interaction with ice shelves of the Amundsen Sea region

The topic of the application problem is to study transmission of ocean waves and tsunamis through the ice shelves of the Amundsen Sea region (Fig. 5) in West Antarctica. For the application problem, we modify the domain (Fig. 6) and utilize a different boundary condition on ϕ . The domain is obtained by approximating Fig. 5. First, we want to enforce a non-reflective boundary condition on the open water part, where the waves leave the current domain without reflection. Second, we want to provide an incoming wave into the system through this boundary. To do this, we divide the whole boundary $\partial\Omega$ into 2 disjoint sub-boundaries: $\partial\Omega = \partial\Omega_{NR} \cup \partial\Omega_{R}$. Neumann boundary conditions are enforced on $\partial\Omega_{R}$ (166a) and non-reflective boundary conditions with incoming incident waves are enforced on $\partial\Omega_{NR}$ (166b):

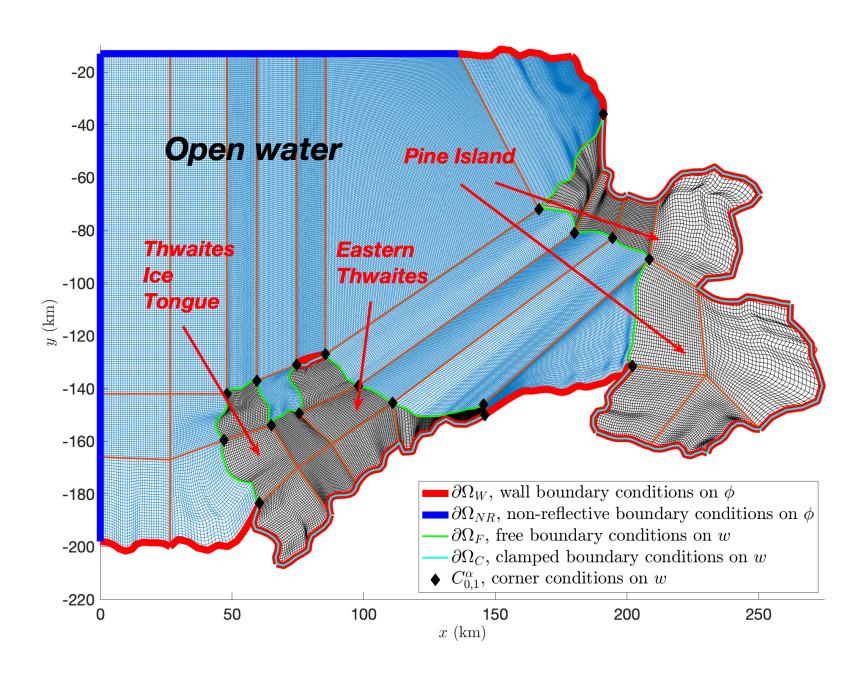


Figure 6: Amundsen Sea region and grid configuration

$$n_I \partial_I \phi = 0,$$
 $\vec{X} \in \partial \Omega_R, \qquad t \ge 0,$ (166a)

$$n_{I}\partial_{I}\phi = 0, \qquad \vec{X} \in \partial\Omega_{R}, \qquad t \geq 0, \qquad (166a)$$

$$\frac{1}{\sqrt{gH}}\dot{\phi} - n_{I}\partial_{I}\phi = \frac{1}{\sqrt{gH}}\dot{\phi}^{(D)} - n_{I}\partial_{I}\phi^{(D)}, \qquad \vec{X} \in \partial\Omega_{NR}, \qquad t \geq 0. \qquad (166b)$$

The non-reflecting condition specifies data for the characteristic variable associated with shallow water waves, propagating at speed \sqrt{gH} , into the domain. For data, we specify an incident plane wave of the form

$$\phi^{(D)}(x,y,t) = \phi_0 e^{-\frac{1}{2} \left(\frac{(t-t_0) - s_x x - s_y y}{T}\right)^2},\tag{167}$$

where $\phi_0 = 0.5$ and $(s_x, s_y) = 1/c \cdot (\cos(\theta), \sin(\theta))$ is the slowness vector, $c = \sqrt{gH}$ is the wave speed (evaluated using local properties), and $\theta = 7\pi/4$ is the angle of the direction of wave propagation counterclockwise from the x-axis. Here T (in seconds) controls the frequencies of the incident wave and $t_0 = 4T$ is for delay. Furthermore, we obtain the variable water depth (Fig. 7a) and ice thickness (Fig. 7c) from BedMachine Version 2 [26]. Next, we interpolate both values over the grid points of Ω (Fig. 7b and 7d). We set Poisson ratio to $\nu = 0.3$.

The simulation results, shown in Figs. 8 and 9 for T=10 s and 30 s, respectively, show an extremely complex wavefield resulting from scattering and diffraction in response to variable water depth, ice thickness, and the complex geometry of the coastline and ice shelf edge. Consistent with previous studies, only sufficiently long wavelength incident waves are transmitted across the ice shelf edge. In addition to providing predictions of the wave amplitude w, our method can be used to quantify the bending moments and shear forces acting within the ice, which can be combined with fracture mechanics concepts to assess the likelihood of rift development and growth.

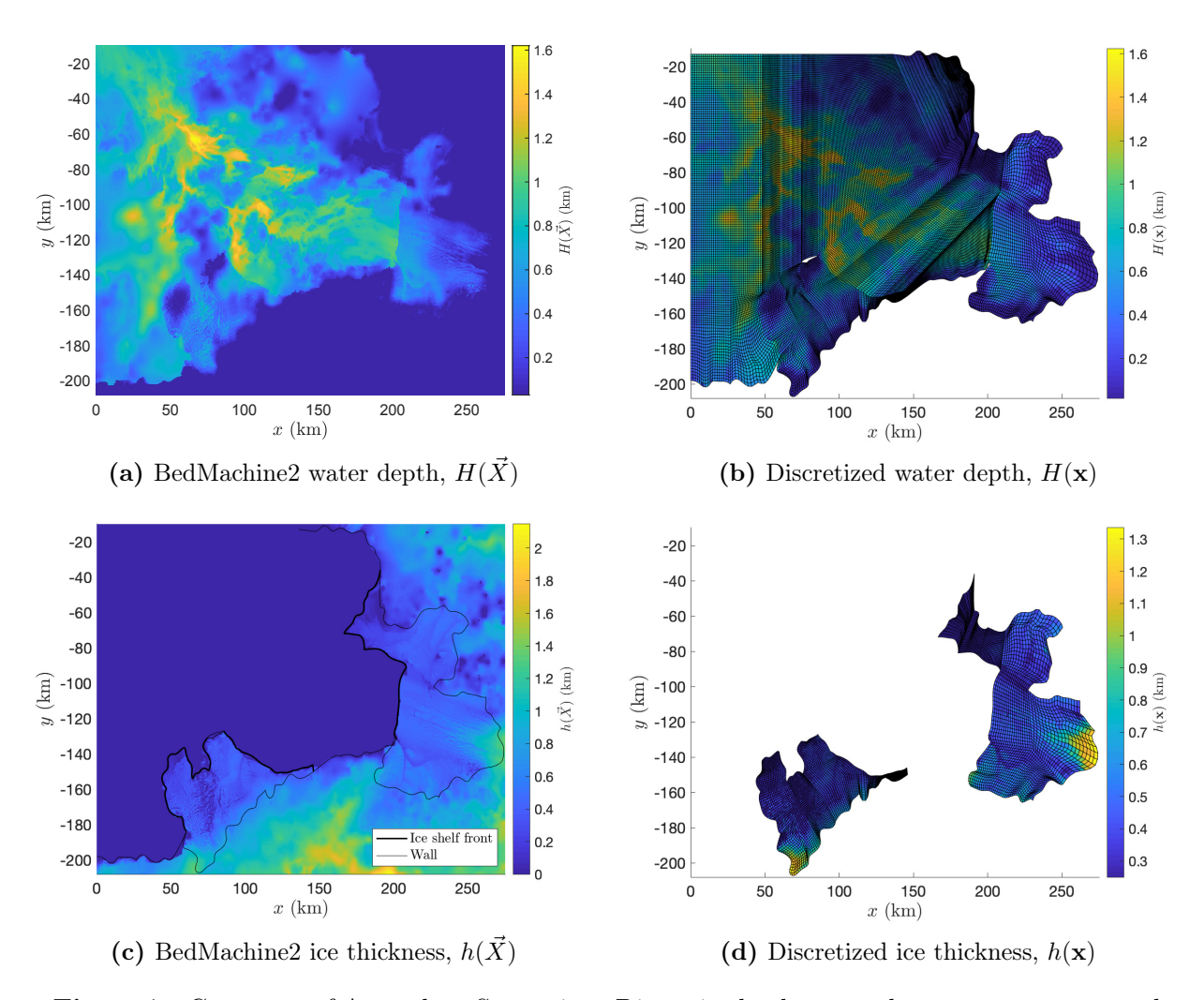


Figure 7: Geometry of Amundsen Sea region. Discretized values are shown on a coarser mesh than used in the simulations for easier visualization.

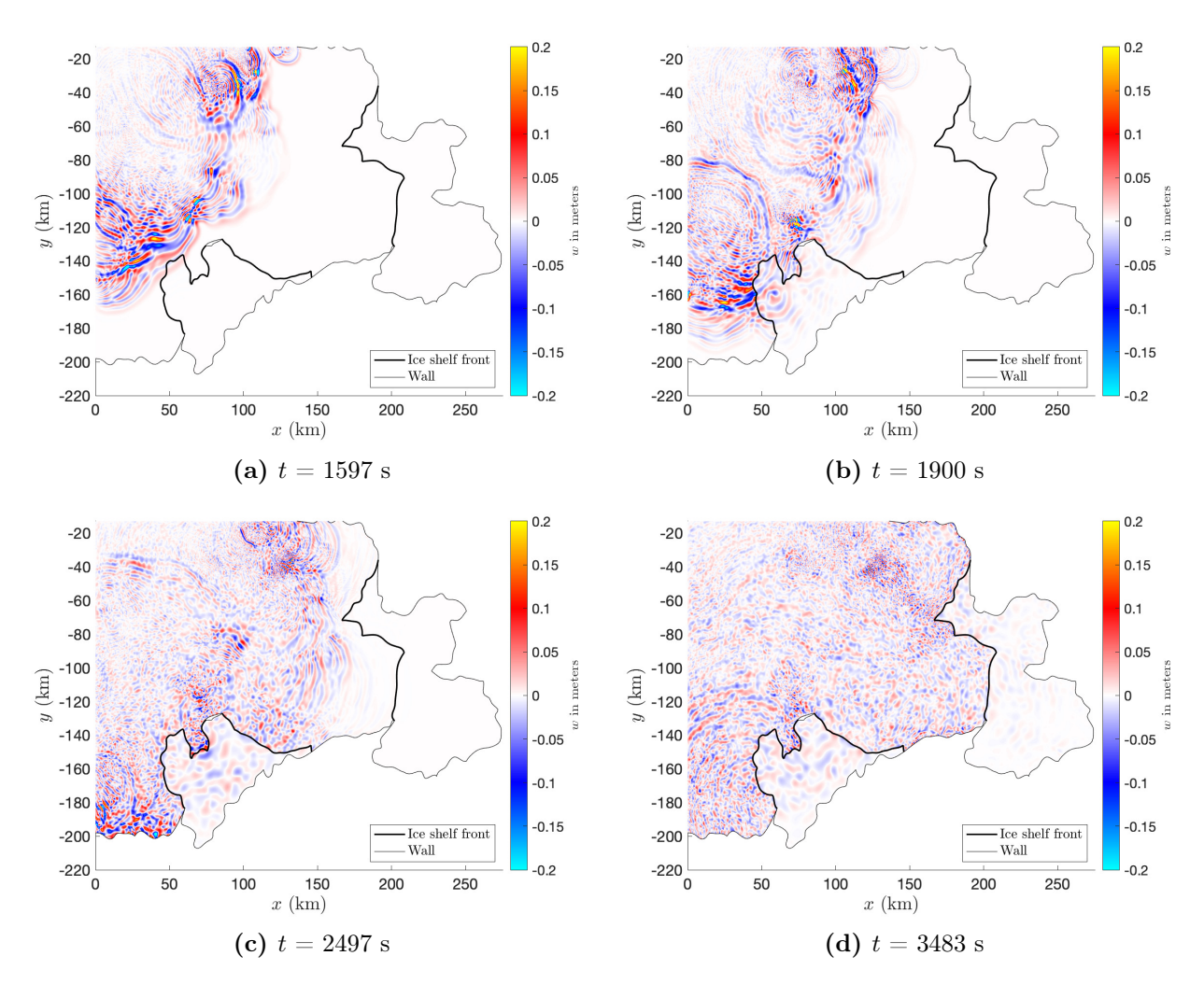


Figure 8: Plots of vertical displacement w in meters for T=10 s. The top two rows show the snapshots of w at different times. (a) Arrival of incident waves at the ice shelf front of Thwaites Ice Tongue at t=1597 s. (b) Reflection from and transmission through the ice shelf front and arrival at grounding zone at t=1900 s. (c) Complex wavefield with reflections and scattering and arrival of incident waves at the Pine Island Ice Shelf at t=2497 s. (d) Larger amplitudes and shorter wavelengths in the ocean, smaller in the ice shelf at t=3483 s.

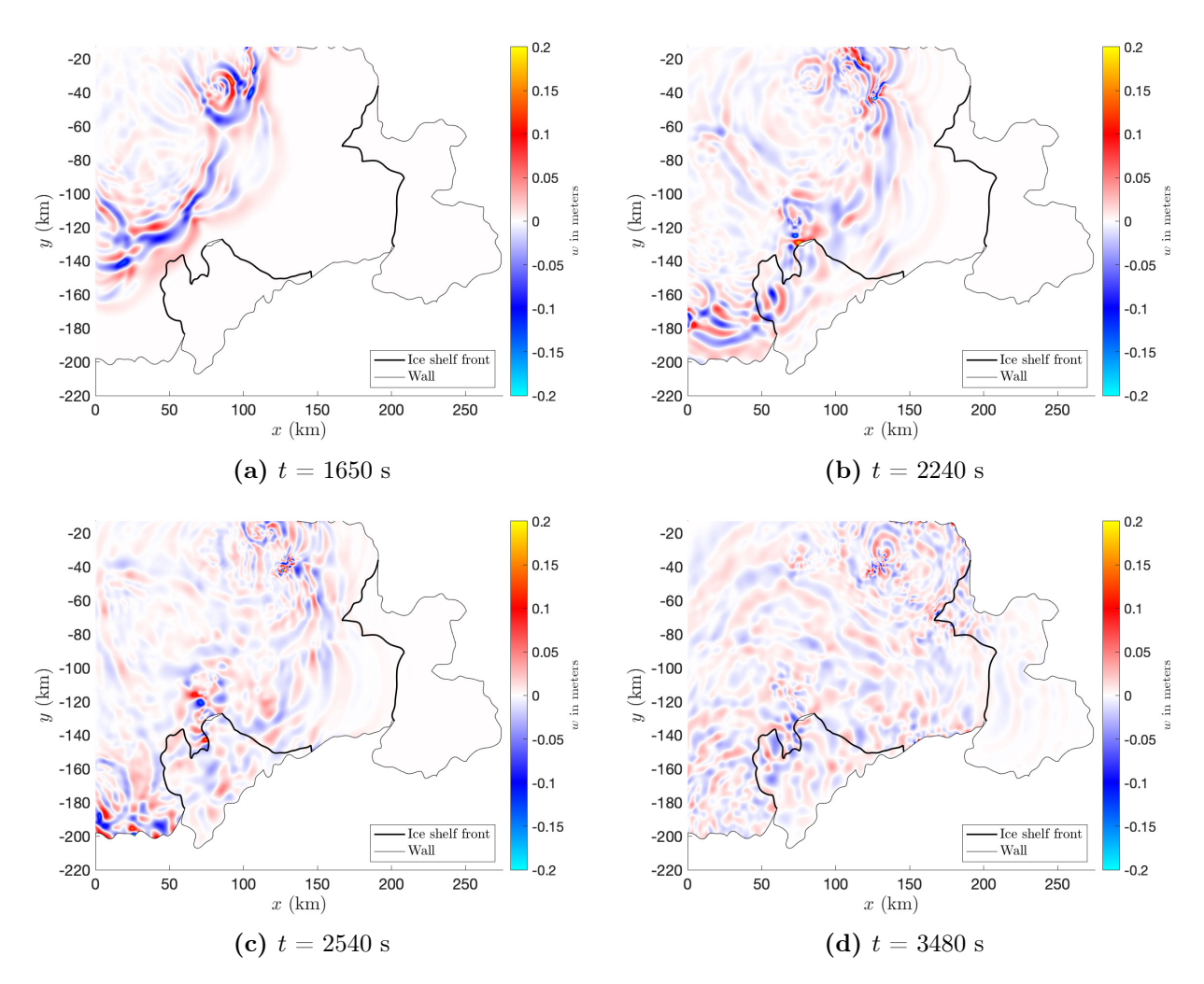


Figure 9: Plots of vertical displacement w in meters for T=30 s. The top two rows show the snapshots of w at different times. (a) Arrival of incident waves at the Thwaites Ice Shelf front at t=1650 s. (b) Reflection from ice shelf front and flexural-gravity waves reach the grounding zone of Thwaites Ice Shelf at t=2240 s. (c) Arrival of waves at the Pine Island Ice Shelf front at t=2540 s. (d) Complex wavefield with scattering at t=3480 s.

9. Conclusions

We have developed an SBP-SAT method for the variable coefficient 2D plate equation on curvilinear multiblock grids. Free boundary and corresponding corner conditions, clamped boundary conditions, and interface conditions are all enforced utilizing SATs, which make the spatial discretization energy-stable and self-adjoint by design. Numerical experiments indicate that the convergence rates are 2, 3.5 and 4.5 for interior orders of two, four and six, respectively.

For the numerical experiments, we formed an ocean-wave-ice-shelf interaction problem for Thwaites Glacier Tongue and Pine Island ice shelves in the Amundsen Sea region off the coast of West Antarctica. Our approach handles variable coefficients and complex geometries, which is essential for modeling real-world problems in the cryosphere. Future simulations can take tsunami and wave data (either from separate simulations or observations) to force the model, in order to quantify the response of ice shelves to forcing from ocean waves and tides. The model can provide predictions of bending stresses and shear forces, which may cause fracturing and even break-up of the ice shelves, and to identify regions in which bending stresses are amplified by wave focusing. In addition, the model could be utilized in the PDE-constrained optimization framework of full waveform inversion, in which model parameters like ice thickness and bending stiffness are adjusted to minimize the misfit between modeled and observed wavefield measurements. The self-adjoint SBP-SAT framework is ideally suited for this class of problems [3].

MATLAB source code that reproduces figures (4), (8), (9) is available at https://www.usap-dc.org/view/dataset/601561.

CRediT authorship contribution statement

Nurbek Tazhimbetov: Conceptualization, Software, Visualization, Writing - original draft. Martin Almquist: Conceptualization, Methodology, Software, Writing - review & editing. Jonatan Werpers: Conceptualization, Software. Eric Dunham: Conceptualization, Funding acquisition, Investigation, Writing - review & editing.

Declaration of competing interest

The authors declare that they have no known competing financial interests or personal relationships that could have appeared to influence the work reported in this paper.

Acknowledgements

M.Almquist gratefully acknowledges support from the Knut and Alice Wallenberg Foundation (Dnr. KAW 2016.0498). This work was also supported by the National Science Foundation (OPP-1744759).

References

- [1] Almquist, M., Dunham, E.M., 2020. Non-stiff boundary and interface penalties for narrow-stencil finite difference approximations of the Laplacian on curvilinear multiblock grids. J. Comput. Phys. 408. URL: https://doi.org/10.1016/j.jcp.2020.109294, doi:10.1016/j.jcp.2020.109294.
- [2] Almquist, M., Dunham, E.M., 2021. Elastic wave propagation in anisotropic solids using energy-stable finite differences with weakly enforced boundary and interface conditions. J. Comput. Phys. 424, 109842. URL: https://doi.org/10.1016/j.jcp.2020.109842, doi:10.1016/j.jcp.2020.109842.
- [3] Bader, M., Almquist, M., Dunham, E., 2021. Acoustic-elastic waveform modeling and inversion using energy-stable summation-by-parts finite-difference operators. First International Meeting for Applied Geoscience & Energy Expanded Abstracts doi:https://doi.org/10.1190/segam2021-3579516.1.
- [4] Bromirski, P., Chen, Z., Stephen, R., Gerstoft, P., Arcas, D., Diez, A., Aster, R., Wiens, D., Nyblade, A., 2017. Tsunami and infragravity waves impacting Antarctic ice shelves. Journal of Geophysical Research.

- [5] Bromirski, P.D., Diez, A., Gerstoft, P., Stephen, R.A., Bolmer, T., Wiens, D.A., Aster, R.C., Nyblade, A., 2015. Ross ice shelf vibrations. Geophysical Research Letters 42, 7589–7597.
- [6] Carpenter, M.H., Gottlieb, D., Abarbanel, S., 1994. Time-stable boundary conditions for finite-difference schemes solving hyperbolic systems: Methodology and application to high-order compact schemes. J. Comput. Phys. 111(2), 220-236. URL: https://doi.org/10.1006/jcph.1994.1057, doi:10.1006/jcph.1994.1057.
- [7] Del Rey Fernández, D.C., Hicken, J.E., Zingg, D.W., 2014. Review of summation-by-parts operators with simultaneous approximation terms for the numerical solution of partial differential equations. Comput. Fluids 95, 171–196. URL: https://doi.org/10.1016/j.compfluid.2014.02.016, doi:10.1016/j.compfluid.2014.02.016.
- [8] Fox, C., Squire, V.A., 1991. Coupling between the ocean and an ice shelf. Annals of Glaciology 15, 101–108.
- [9] Holdsworth, G., Glynn, J., 1978. Iceberg calving from floating glaciers by a vibrating mechanism. Nature 274, 464–466.
- [10] Holdsworth, G., Glynn, J., 1981. A mechanism for the formation of large icebergs. Journal of Geophysical Research 86, 3210. URL: doi:10.1029/jc086ic04p03210.
- [11] Ilyas, M., Meylan, M.H., Lamichhane, B., Bennetts, L.G., 2018. Time-domain and modal response of ice shelves to wave forcing using the finite element method. Journal of Fluids and Structures 80, 113–131. URL: https://doi.org/10.1016/j.jfluidstructs.2018.03.010.
- [12] Kalyanaraman, B., Bennetts, L.G., Lamichhane, B., Meylan, M.H., 2019. On the shallow-water limit for modelling ocean-wave induced ice-shelf vibrations. Wave Motion 90, 1–16.
- [13] Kalyanaraman, B., Meylan, M.H., Bennetts, L.G., Lamichhane, B.P., 2020. A coupled fluid-elasticity model for wave forcing of an ice-shelf. J. Fluids Struct. 97, 103074.
- [14] Kircchoff, G., 1850. Uber das gleichgewicht und die bewegung einer elastischen scheibe. J. Reine Angew. Math. 40, 51–88.
- [15] Kreiss, H.O., Oliger, J., 1972. Comparison of accurate methods for the integration of hyperbolic equations. Tellus XXIV, 199-215. URL: https://doi.org/10.3402/tellusa.v24i3.10634, doi:10.3402/tellusa.v24i3.10634.
- [16] Kreiss, H.O., Scherer, G., 1974. Finite element and finite difference methods for hyperbolic partial differential equations. Mathematical Aspects of Finite Elements in Partial Differential Equations., Academic Press, Inc. , 195–212URL: https://doi.org/10.1016/B978-0-12-208350-1.50012-1, doi:10.1016/B978-0-12-208350-1.50012-1.
- [17] Lamb, H., 1889. On the flexure of an elastic plate. Proc. London Math. Soc. 21, 70–91.
- [18] MacAyeal, D.R., Okal, E.A., Aster, R.C., Bassis, J.N., Brunt, K.M., Cathles, L.M., Drucker, R., Fricker, H.A., Kim, Y.J., Martin, S., Okal, M.H., Sergienko, O.V., Sponsler, M.P., Thom, J.E., 2006. Transoceanic wave propagation links iceberg calving margins of antarctica with storms in tropics and northern hemisphere. Geophysical Research Letters 33.
- [19] Malvern, L.E., 1969. Introduction to the Mechanics of a Continuous Medium. Prentice-Hall, Inc.
- [20] Massom, R.A., Scambos, T.A., Bennetts, L.G., Reid, P., Squire, V.A., Stammerjohn, S.E., 2018. Antarctic ice shelf disintegration triggered by sea ice loss and ocean swell. Nature 558(7710), 383–389.
- [21] Mattsson, K., 2012. Summation by parts operators for finite difference approximations of second-derivatives with variable coefficients. J. Sci. Comput 51, 650–682. doi:DOI10.1007/s10915-011-9525-z.
- [22] Mattsson, K., 2014. Diagonal-norm summation by parts operators for finite difference approximations of third and fourth derivatives. J. Comput. Phys. 274, 432 454. URL: http://www.sciencedirect.com/science/article/pii/S0021999114004343, doi:http://dx.doi.org/10.1016/j.jcp.2014.06.027.
- [23] Mattsson, K., Dunham, E.M., Werpers, J., 2018. Simulation of acoustic and flexural-gravity waves. J. Comput. Phys. 373, 230-252. URL: https://doi.org/10.1016/j.jcp.2018.06.060, doi:10.1016/j.jcp.2018.06.060.
- [24] Mattsson, K., Stiernström, V., 2015. High-fidelity numerical simulation of the dynamic beam equation. Journal of Computational Physics 286, 194 213. URL: http://www.sciencedirect.com/science/

- article/pii/S0021999115000522, doi:http://dx.doi.org/10.1016/j.jcp.2015.01.038.
- [25] Meylan, M.H., Ilyas, M., Lamichhane, B.P., Bennetts, L.G., 2021. Swell-induced flexural vibrations of a thickening ice shelf over a shoaling seabed. Proceedings of the Royal Society A 477: 20210173. URL: https://doi.org/10.1098/rspa.2021.0173.
- [26] Morlighem, M., Rignot, E., Binder, T., Blankenship, D.D., Drews, R., Eagles, G., Eisen, O., Ferraccioli, F., Forsberg, R., Fretwell, P., Goel, V., Greenbaum, J.S., Gudmundsson, H., Guo, J., Helm, V., Hofstede, C., Howat, I., Humbert, A., Jokat, W., Karlsson, N.B., Lee, W., Matsuoka, K., Millan, R., Mouginot, J., Paden, J., Pattyn, F., Roberts, J.L., Rosier, S., Ruppel, A., Seroussi, H., Smith, E.C., Steinhage, D., Sun, B., van den Broeke, M.R., van Ommen, T., van Wessem, M., Young, D.A., 2020. Deep glacial troughs and stabilizing ridges unveiled beneath the margins of the antarctic ice sheet. Nature Geoscience 13, 132–137. URL: https://doi.org/10.1038/s41561-019-0510-8.
- [27] Papathanasiou, T.K., Karperaki, A.E., Theotokoglou, E.E., Belibassakis, K.A., 2015. Hydroelastic analysis of ice shelves under long wave excitation. Natural Hazards and Earth System Sciences 15, 1851–1857. URL: http://www.nat-hazards-earth-syst-sci.net/15/1851/2015/, doi:10.5194/nhess-15-1851-2015.
- [28] Petersson, N.A., Sjögreen, B., 2015. Wave propagation in anisotropic elastic materials and curvilinear coordinates using a summation-by-parts finite difference method. J. Comput. Phys. 299, 820–841. URL: http://dx.doi.org/10.1016/j.jcp.2015.07.023, doi:10.1016/j.jcp.2015.07.023.
- [29] Reddy, J.N., 2007. Theory and Analysis of Elastic Plates and Shells. CRC Press.
- [30] Rudin, W., 1973. Functional Analysis. McGraw-Hill Book Company.
- [31] Sergienko, O., 2010. Elastic response of floating glacier ice to impact of long-period ocean waves. Journal of Geophysical Research 115.
- [32] Sergienko, O., 2017. Behavior of flexural gravity waves on ice shelves: Application to the ross ice shelf. Journal of Geophysical Research: Oceans .
- [33] Sturova, I.V., 2009. Time-dependent response of a heterogeneous elastic plate floating on shallow water of variable depth. Journal of Fluid Mechanics 637, 305–325.
- [34] Svärd, M., Nordström, J., 2014. Review of summation-by-parts schemes for initial-boundary-value problems. J. Comput. Phys. 268, 17–38. URL: https://doi.org/10.1016/j.jcp.2014.02.031, doi:10.1016/j.jcp.2014.02.031.
- [35] Thompson, J.F., Warsi, Z.U., Mastin, C.W., 1985. Numerical grid generation: foundations and applications. volume 45. North-holland Amsterdam. URL: http://www.hpc.msstate.edu/publications/gridbook/cover.php.